Lithos 324–325 (2019) 115–140

Contents lists available at ScienceDirect

Lithos

journal homepage: www.elsevier.com/locate/lithos

Early Palaeozoic metamorphism of Precambrian crust in the Zheltau terrane (Southern Kazakhstan; Central Asian Orogenic belt): P-T paths, protoliths, zircon dating and tectonic implications

A.V. Pilitsyna [a,*], A.A. Tretyakov [a], K.E. Degtyarev [a], E.B. Salnikova [b], A.B. Kotov [b], V.P. Kovach [b], K.-L. Wang [c], V.G. Batanova [d,e], Yu.V. Plotkina [b], E.V. Tolmacheva [b], B.V. Ermolaev [a], H.-Y. Lee [c]

[a] Geological Institute, Russian Academy of Sciences, Pyzhevsky lane, 7a, Moscow, Russia
[b] Institute of Precambrian geology and Geochronology, Russian Academy of Sciences, Makarova emb. 2, Saint Petersburg, Russia
[c] Institute of Earth Sciences, Academia Sinica, P.O. Box 1-55, Nangang, Taipei 11529, Taiwan
[d] Univ. Grenoble Alpes, Univ. Savoie Mont Blanc, CNRS, IRD, IFSTTAR, ISTerre, 38000 Grenoble, France
[e] Vernadsky Institute of Geochemistry and Analytical Chemistry, Russian Academy of Sciences, Kosygin str, 19 Moscow, Russia

ARTICLE INFO

Article history:
Received 30 March 2018
19 October 2018
Accepted 30 October 2018
Available online 07 November 2018

Keywords:
Central Asian orogenic belt
Continental crust
Zircon dating
Sm-Nd isotope systematics
P-T path
High-pressure granulite

ABSTRACT

Palaeoproterozoic amphibole-biotite orthogneisses with a protolith age of ~ 1840 Ma and Neoproterozoic muscovite-chlorite orthogneisses with an estimated protolith age of ~ 790 Ma have been identified in the structure of the Zheltau terrane (Southern Kazakhstan; west Central Asian Orogenic belt). In addition, metasedimentary complexes represented by prevailing garnet-mica schists and subordinate muscovite-chlorite schists with obtained detrital zircon ages in the range of 604 - 2819 Ma (with two peaks at ~ 991 Ma and ~ 1082 Ma) also comprise the Zheltau terrane. In accordance with the Sm-Nd whole-rock isotopic compositions, the protolith of the observed Palaeoproterozoic orthogneisses formed as a result of a mixing of the Neoarchean crustal source with a juvenile source, whereas the formation of the Neoproterozoic orthogneisses protolith may have been related to the melting of Palaeoproterozoic crustal material. In turn, Late Mesoproterozoic – Early Neoproterozoic granitoids or felsic volcanic rocks, which formed as a result of the melting of Palaeoproterozoic continental crust, are considered as possible sources for the studied detrital zircons obtained from the schists. The terrigenous protolith of the schists from the Zheltau terrane accumulated in the range of ~ 600 to ~ 490 Ma, corresponding to the Ediacaran-Cambrian. Subduction processes in the Early Palaeozoic led to the burial of different horizons of the Zheltau terrane continental crust to significant depths; some of the complexes experienced high-pressure metamorphism at P 15 – 18 kbar; T 750 – 850 °C (high-pressure granulites), whereas most of the rocks were evidently metamorphosed at maximum amphibolite facies and avoided high-pressure re-equilibration. The spatial proximity of the studied metamagmatic and metasedimentary crustal complexes and similar metamorphic changes during the latest stages of retrogression imply their possible mutual exhumation from different levels during the period between 490 and 470 Ma and their following juxtaposition as a package of tectonic slices.

1. Introduction

The Central Asian Orogenic Belt (CAOB) represents the largest contractional orogen and is framed by the Siberian, North China and Tarim cratons. The formation of continental crust in the CAOB took more than one billion years from the Neoproterozoic to Mesozoic (Mossakovsky et al., 1993; Sengör et al., 1993; Windley et al., 2007; Zonenshain et al., 1990). A significant volume of continental crust of the CAOB was produced during the Late Precambrian-Early Palaeozoic at the expense of juvenile crust transformation. Moreover, in the structure of the CAOB, older complexes, comprising large terranes, are present; a profound study of these terranes is a key to understanding the earlier stages of continental crust of the CAOB formation. In the western part of the CAOB, the terranes comprise thick terrigenous, quartzite-schist, felsic volcanic and igneous complexes, the formation of which occurred from the Late Mesoproterozoic to Early Neoproterozoic (1200–900 Ma) (Kozakov, 1993; Letnikov et al., 2007; Kröner et al., 2007, 2012; Degtyarev et al., 2014, Degtyarev, 2012; Levashova et al., 2007; Turkina et al., 2011; Tretyakov et al., 2011a, 2011b). The data obtained in the last several years on the ages of detrital zircons and Sm—Nd whole-rock isotopic compositions of Meso- to Neoproterozoic quartzite-

* Corresponding author.
E-mail addresses: an.pilitsyna@gmail.com (A.V. Pilitsyna), klwang@gate.sinica.edu.tw (K.-L. Wang), valentina.batanova@univ-grenoble-alpes.fr (V.G. Batanova), analytic@ginras.ru (B.V. Ermolaev), haoyanglee@earth.sinica.edu.tw (H.-Y. Lee).

https://doi.org/10.1016/j.lithos.2018.10.033
0024-4937/

schists, granitoids and volcanic rocks indicate that their formation was related to the intracrustal recycling and reworking of older continental crust (Kröner et al., 2007, 2012, 2013; Rojas-Agramonte et al., 2014; Tretyakov et al., 2016a, 2016b; Degtyarev et al., 2017; Kovach et al., 2017). Hence, the overwhelming volume of continental crust in the terranes of the western part of the CAOB was formed in the pre-Mesoproterozoic. However, in the modern erosion zone, the pre-Mesoproterozoic complexes are poorly developed (Kröner et al., 2007, 2017, Tretyakov et al., 2016a), which may have been related to either their complete erosion or their placement in the structure of the deeper horizons of continental crust of the terranes. A number of terranes in the western CAOB (e.g., Kokchetav, Chu-Kendyktas, Issyk-Kul, etc. (Fig. 1, A)) are characterized by the presence of metamorphic complexes of high-pressure (HP) and ultrahigh-pressure (UHP) origin; in the structures of these complexes, metamorphic formations with a long crustal prehistory are prevalent (Shatsky et al., 1999; Kröner et al., 2007, 2012; Alexeiev et al., 2011; Konopelko et al., 2012; Degtyarev et al., 2014, Degtyarev et al., 2017; Rojas-Agramonte et al., 2014; Tretyakov et al., 2016b). Therefore, HP and UHP complexes provide perspective for the identification and investigation of Precambrian crustal complexes.

The first data on high-pressure metamorphic formations within the Zheltau terrane in Southern Kazakhstan were provided in Efimov et al. (1983), where eclogites among garnet-bearing mica schists were superficially described. However, the detailed information on mineral compositions and metamorphic evolution of the high-pressure complexes was absent. In the following works of Alexeiev et al. (2011), Pilitsyna et al. (2018a, 2018b), the ages, protolith sources and P-T paths for ultramafic and mafic high-pressure rocks of the terrane, including eclogites, garnet clinopyroxenites, spinel peridotites, were considered. Nevertheless, the most widespread quartz-feldspar metamorphic formations of the Zheltau terrane, in many cases enclosing pods of HP ultramafic/mafic lithologies, were poorly investigated so far. In the present paper, the new results of U—Pb and U-Th-Pb geochronological studies as well as Sm—Nd whole-rock isotopic investigations of metamorphic quartz-feldspar crustal complexes of the Zheltau terrane are provided. It is shown that in the structure of the Zheltau terrane, Palaeoproterozoic and Neoproterozoic crustal complexes are present. Moreover, it has been justified for the first time that at least part of the Precambrian crustal complexes experienced high-pressure metamorphism in the Late Cambrian-Early Ordovician. Petrological observations together with geothermobarometry estimations displayed the "clockwise" P-T path for the studied complexes, which is thought to be a common scenario for high-pressure rocks, formed in subduction-collision settings (e.g. Faryad, 2011; Li et al., 2015). Thus, the formation of the high-pressure complexes of the Zheltau terrane is considered to have been related to the subduction of different horizons of Precambrian crust to high-grade conditions and their subsequent relatively fast exhumation to upper crustal levels.

Provided comprehensive studies of the metamagmatic and metasedimentary formations of the Zheltau terrane allowed to

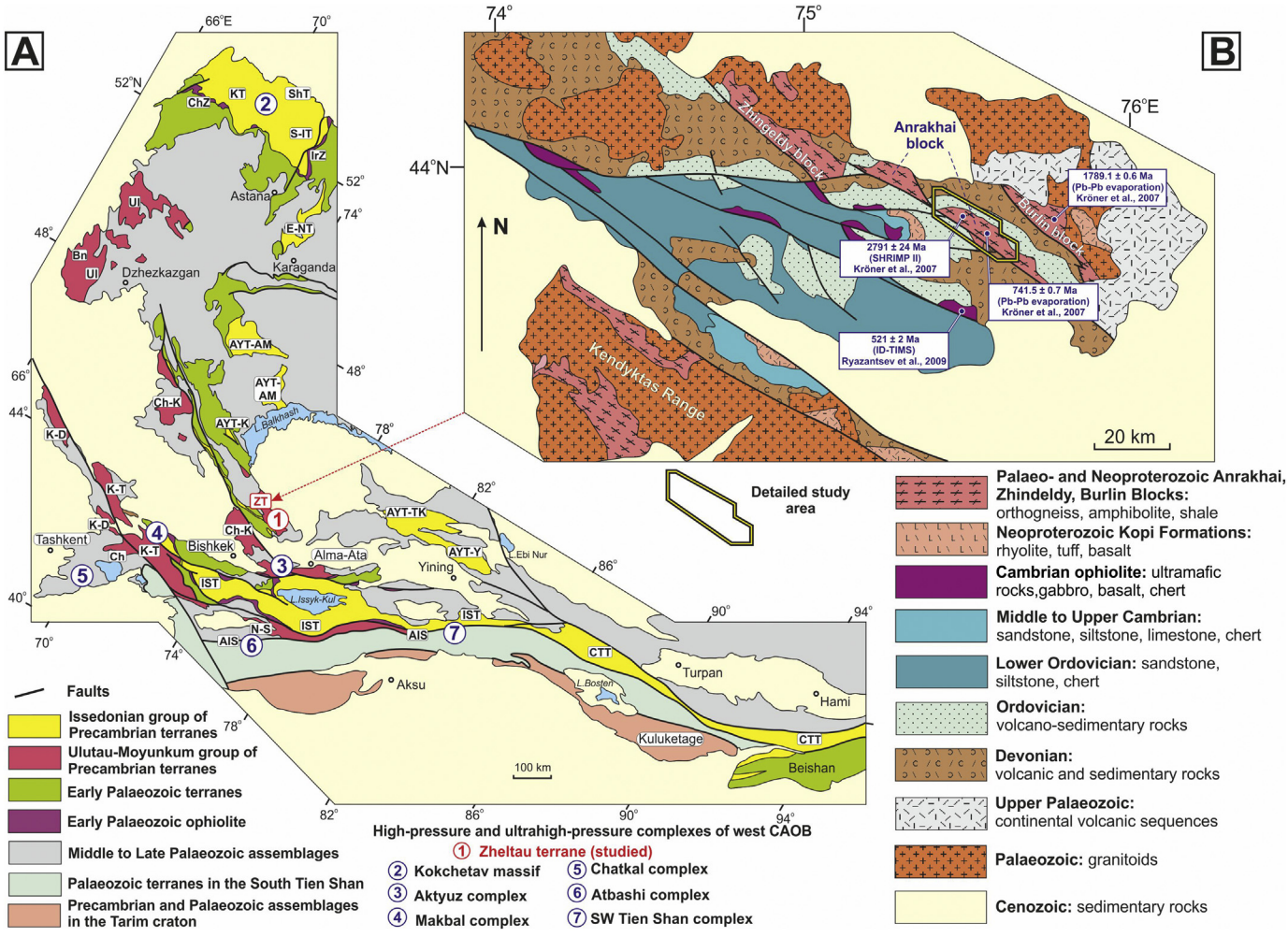

Fig. 1. A. Precambrian terranes of the western CAOB: AYT – Aktau-Yili (AYT-AM – Aktau-Mointy, AYT-K – Karakamys, AYT-TK – Tekeli, AYT-Y – Yili areas), CTT – Chinese Central Tien Shan, E-NT – Erementau-Niyaz, IST – Issyk-Kul, KT – Kokchetav, ShT – Shatskiy, S-IT – Stepnyak-Ishkeolmes, ZT – Zheltau. Subterranes in the Ulutau-Sarydzhaz terrane: Bn – Baikonur, Ch – Chatkal, Ch-K – Chu-Kendyktas, K-D – Karatau-Dzhebagly, K-T – Karatau-Talas, N—S – Naryn-Sarydzhaz, Ul – Ulutau. AIS – Atbashi-Inylchek suture (after Degtyarev et al., 2017). B. Geological map of the SE part of the Chu-Ili Mountains.

reconstruct Precambrian evolution and palaeotectonic position of the terrane in Precambrian, recover P-T-t paths of metamorphism of the rocks and compare the obtained data with those, resulted from the well-studied metamorphic complexes of the adjacent Chu-Kendyktas terrane with the Aktyuz high-pressure complex (described in details in Tagiri et al. (1995); Orozbaev et al. (2010); Kröner et al. (2012); Klemd et al. (2014); among others) (Fig. 1, A).

In the structure of the Zheltau terrane Early Precambrian complexes (which are extremely rare for the western CAOB) and Late Precambrian complexes as well as metamagmatic and metasedimentary formations of high-pressure origin together with fragments of ophiolites are present. This could shed light on evolution of formation and transformation of continental crust in the CAOB during a wide period (from Paleoproterozoic to Early Palaeozoic) within the scope of the relatively small terrane.

2. Geological background

The Precambrian terranes of the western part of the CAOB, which include the Kazakh Uplands, Tien-Shan and NW China, comprise approximately 50% of its crust and mainly consist of Mesoproterozoic and Neoproterozoic magmatic and sedimentary rocks (Degtyarev et al., 2017). The terranes represent isolated areas of various sizes, generally forming narrow (150–200 km) tectonic zones up to 2600 km long. Normally, the Precambrian terranes are separated from each other by Early Palaeozoic accretionary wedge and island arc complexes as well as dismembered ophiolitic associations (Fig. 1, A). On the basis of the ages of the magmatic and sedimentary rocks, their structural interrelationships and differences in Mesoproterozoic and Neoproterozoic tectonomagmatic evolution, the Precambrian terranes of the western CAOB, have been divided into the Issedonian (north-eastern) and Ulutau-Moyunkum (south-western) groups (Degtyarev et al., 2017). The studied complexes of the Issedonian group are attributed to the Kokchetav, Aktau-Yili, Issyk-Kul, and Chinese Central Tien Shan terranes, among others, whereas the Ulutau-Moyunkum group generally includes the Karatau, Chu-Kendyktas, Ulutau, Zheltau and other terranes. In many cases, metamorphic complexes with relics of UHP and HP assemblages are preserved among the lithologies of the Precambrian terranes e.g., the Zerendy series of the Kokchetav terrane (diamondiferous paragneisses with bodies of eclogites, spinel and garnet peridotites (Katayama et al., 2001; Kushev and Vinogradov, 1978; Okamoto et al., 2000; Shatsky et al., 1999; Zhang et al., 1997)), the Makbal complex of the Issyk-Kul terrane (glaucophane-bearing and garnet-chloritoid-talc schists with eclogites (Meyer et al., 2013; Rojas-Agramonte et al., 2013; Togonbaeva et al., 2009), and the Aktyuz complex of the Chu-Kendyktas terrane (paragneisses with bodies of eclogites (Klemd et al., 2014; Kröner et al., 2012; Orozbaev et al., 2010; Rojas-Agramonte et al., 2013; Tagiri et al., 1995)), among others). The metamorphic complexes are interpreted to have been formed during the subduction of different horizons of Precambrian lithosphere to eclogite-facies conditions and represent tectonic slice packages exhumed from different levels in the Early Palaeozoic (Katayama et al., 2001; Kröner et al., 2007; Alexeiev et al., 2011; Kröner et al., 2012; Klemd et al., 2014, etc.).

The Zheltau terrane is one of the smallest of those described in the western CAOB and represents a narrow (<30 km) fault-bounded tectonic block extended to the NW by 150–200 km. In the SW, the Zheltau terrane is separated from the Chu-Kendyktas terrane by the Early Palaeozoic Dzhalair-Naiman ophiolite zone, which consists of tectonically accreted Early Cambrian ultramafites, gabbroids, plagiogranites, basalt-rhyolite formations and Late Cambrian tuffaceous silicic formations, overlain by Early Ordovician flyshoid and silicic terrigenous strata (Degtyarev, 2012; Ryazantsev et al., 2009) (Fig. 1, B). The Zheltau terrane includes several blocks (Anrakhai, Zhingeldy and Burlin (Fig. 1, B)) that are separated by Ordovician and Devonian sedimentary or volcanic complexes. We have studied the Anrakhai block, composed of the metamorphic formations of the Anrakhai Complex (AC) and the Koyandy Complex (KC), fragments of dismembered ophiolites and unmetamorphosed granitoids (Kozakov, 1993; Alexeiev et al., 2011). Indicated formations of the Anrakhai block are overlain by Early Ordovician and Middle-to-Late Ordovician terrigenous formations with carbonates (Nedovizin, 1961; Tolmacheva, 2014).

2.1. The Anrakhai Complex (AC): geological outline and sampling

The AC makes up most of the Zheltau terrane, comprising the cognominal Anrakhai and Zhingeldy and Burlin blocks (Fig. 1, B). The AC mainly consists of muscovite-chlorite orthogneisses and amphibolites. Kröner et al. (2007) has obtained different U—Pb age estimates from the orthogneisses. Four zircon grains from the Anrakhai block orthogneisses (near Koyandysai river) were analysed (SHRIMP II), and discordia with two intersections with concordia were obtained. The upper intercept age (2791 ± 24 Ma) is interpreted as the time of the gneisses' protolith formation, whereas the younger age (lower intersection; 1661 ± 43 Ma) is considered to have been related to Pb-loss.

Four zircon grains from the Burlin block (Fig. 1, B) were also analysed (Pb-evaporation technique (Kober, 1986)); the obtained $^{207}Pb/^{206}Pb$ age of 1789.1 ± 0.6 Ma is thought to reflect the protolith age (Kröner et al., 2007). Zircons from the orthogneisses of the Anrakhai block (near the Ashchisu river) yielded a $^{207}Pb/^{206}Pb$ age of 741.5 ± 0.7 Ma (Pb-evaporation technique (Kober, 1986)), which has been interpreted as the time of gneisses' protolith emplacement (Kröner et al., 2007).

In addition, among the muscovite-chlorite orthogneisses of the AC subalkaline, reddish varieties, represented by amphibole-biotite orthogneisses, are exposed (Fig. 2). The latter possess a subordinate distribution in comparison to the abundant muscovite-chlorite orthogneisses; they also contain pods of subalkaline amphibolites.

Despite the evident profound study of the ages of the metamagmatic complexes' formation in the AC provided by Kröner et al. (2007), it must be cautioned that these data were mostly obtained with the Pb-evaporation technique (Kober, 1986) and therefore could be considered to be preliminary. Consequently, U—Pb data on the ages of the orthogneisses' protolith formation remain of great interest.

Our study has shown that in the SW part of the AC amphibolites (± garnet) are predominant; they contain bodies of muscovite-chlorite orthogneisses of various size (Fig. 2), whereas in the SE part, the Complex is mostly composed of muscovite-chlorite orthogneisses with sporadic bodies of amphibolites (Fig. 2, a). The orthogneisses together with amphibolites are deformed into recumbent isoclinal folds. In the SE part of the Anrakhai block the orthogneisses of the AC are pervasively mylonitized and possibly migmatized. However, robust evidences of dehydration partial melting of the orthogneisses with the following diatexite formation are nearly absent due to extremely difficult interrelationships between the metamagmatic and metasedimentary quartz-feldspar complexes in this part of the block. Additional structural and petrological studies of these varieties with identification of migmatized complexes are of great importance.

Banded fine-to-medium grained muscovite-chlorite orthogneisses from the NE part of the Anrakhai block were sampled for the U—Pb dating (TS 1185; Fig. 2, Table 1). In the central part of the Anrakhai block among the muscovite-chlorite orthogneisses a tectonic slice of intensively deformed amphibole-biotite orthogneisses with sparse bodies of amphibolites is present. The amphibole-biotite orthogneisses of the AC were also sampled for the U—Pb dating (Z 12371; Fig. 2, Table 1).

2.2. The Koyandy Complex (KC): geological outline and sampling

From the NE, the AC has been overthrust by the metamorphic formations of the KC, forming a narrow tectonic slice of NW-trending, with its breadth ranging from 50 m to 1.5 km. The predominant metamorphic formations of the KC are metasedimentary rocks (metapelites), mainly represented by garnet-mica schists with relics of kyanite, phengite

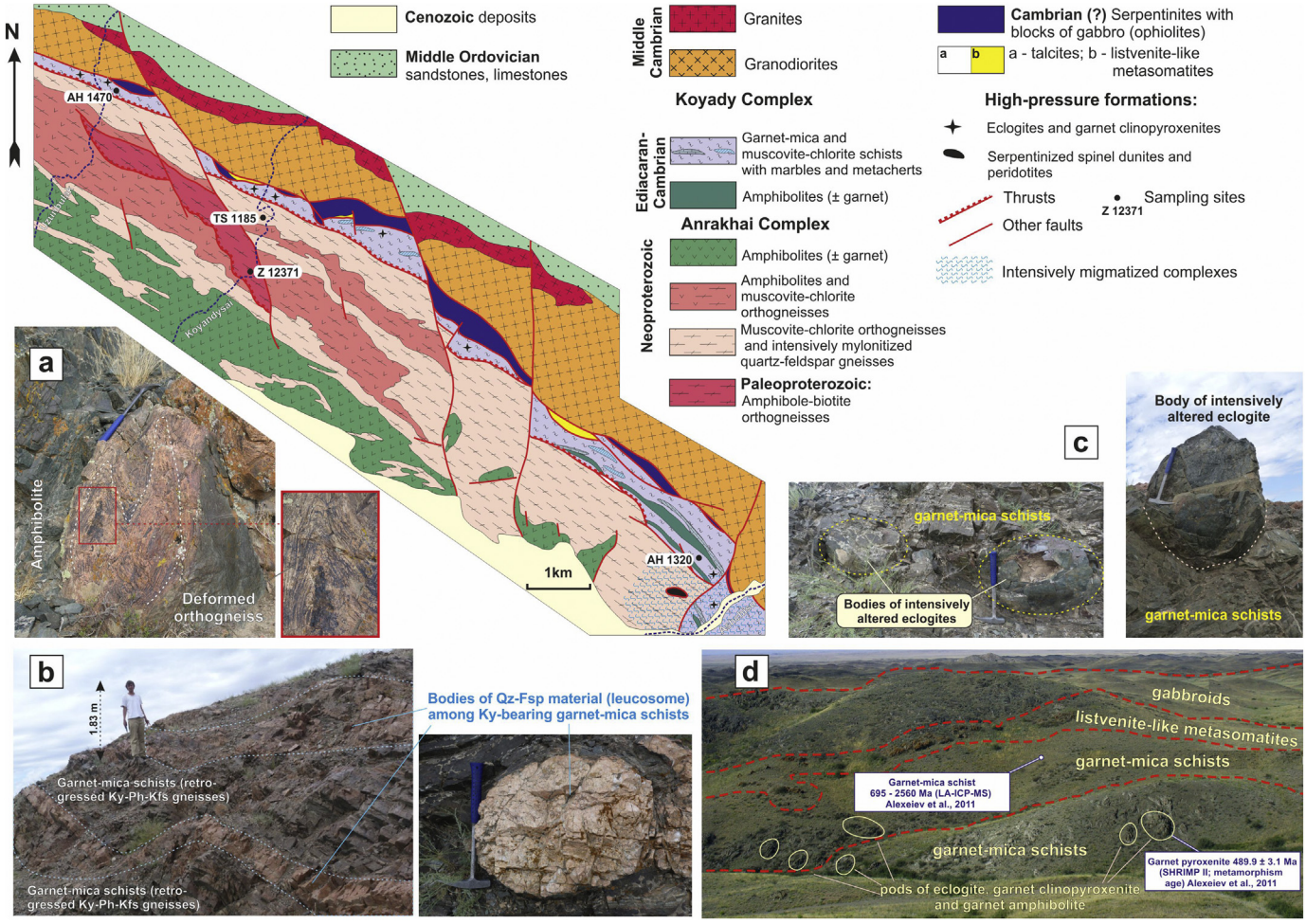

Fig. 2. Geological map of the Anrakhai Mountains. Sample numbers correspond to those, indicated in Tables 1, 2. a) Body of the deformed orthogneiss among amphibolites in the AC; b) migmatized formations of the KC; c) pods of high-pressure rocks among the garnet-mica schists of the KC; d) photo of the NW part of the Anrakhai block.

Table 1
Summary of sample localities, rock types, geological associations, and zircon ages for rocks from the Anrakhai block of the Zheltau terrane.

Sample	N. latitude	E. longitude	Locality	Rock type	Complex/formation	Age (Ma)
Z 12371	43°52′48,2″	75°27′16,2″	Headstream of r. Koyandysai	Amphibole-biotite orthogneisses	Anrakhai Complex	1841 ± 6
TS 1185	43°53′31,7″	75°27′15,3″	Headstream of r. Koyandysai	Muscovite-chlorite orthogneisses	Anrakhai Complex	779 ± 10
AH 1470	43°54′40,6″	75°25′26,8″	Midstream of r. Uzunbulak	Garnet-mica schists	Koyandy Complex	599 to 3582
AH 1320	43°50′29,2″	75°32′28,5″	Left bank of r. Ashchisu	Muscovite-chlorite schists	Koyandy Complex	602 to 3094

and K-feldspar (strongly retrogressed paragneisses) (Fig. 2). Previously, sixteen grains of detrital zircons from the garnet-mica schists near the Koyandysai river were analysed (LA-ICP-MS), and the obtained ages ranged from 694 ± 7 to 2557 ± 27 Ma (Alexeiev et al., 2011). It is noteworthy that the analysed zircons were characterized by the presence of tiny uranium-poor rims that may have been formed during metamorphism. However, these were considered by Alexeiev et al. (2011) as being too narrow to be dated. Hence, additional studies of detrital zircons from the mica schists of the KC with more representative statistics of the grain numbers are obviously needed. Apart from the observed above garnet-mica schists muscovite-chlorite schists without garnet are also present in the structure of the KC. Both types of the schists are associated with sparse bodies of marbles and metacherts (Fig. 2). The garnet-mica schists and muscovite-chlorite schists were sampled for the U-Th-Ph dating of detrital zircons (AH 1470 and AH 1320, respectively; Fig. 2, Table 1).

It has to be added that in some cases evidences of high-grade dehydration melting of garnet-mica schists (retrogressed paragneisses) are present. In the SE part of the Anrakhai block the garnet-bearing mica schists with relics of kyanite, phengite and K-feldspar are virtually diatexites and are characterized by the presence of injections and bands of leucocratic granitic material (leucosome) (Fig. 2, b). However, in the rest part of the block these features are strongly obscured by later processes of retrogression and mylonitization.

2.3. Ultramafic and mafic metamorphic formations

The garnet-mica schists of the KC contain pods and bodies of different sizes (from the first decimeters up to several hundreds of metres) of amphibolites (± garnet), eclogites, garnet clinopyroxenites and intensively altered eclogites (garnetites) (Fig. 2, c, d). In the SE part of the Anrakhai block among the mylonitized and migmatized (?) orthogneisses of the AC large bodies (up to 200 m in size) of garnet amphibolites with lenses of serpentinites or talcites (monomineralic talc rocks) are exposed. Furthermore, serpentinites with relics of spinel peridotites are also present (Fig. 2).

Partially serpentinized spinel peridotites and eclogites/garnet clinopyroxenites have been investigated in detail. Zircons from the garnet clinopyroxenites were analysed, and the obtained age (489.9 ± 3.1 Ma) is interpreted as the time of high-pressure metamorphism (Alexeiev et al., 2011). The rocks are considered to have been derived from the differentiated intraplate tholeiitic melts that were introduced into continental crust prior to subduction (Pilitsyna et al., 2018a, 2018b). The eclogites and garnet clinopyroxenites correspond to the "crustal" type of high-pressure ultramafic-mafic rocks (in accordance with Carswell et al. (1983)). Alternatively, the identified spinel-bearing ultramafic rocks evidently represent a part of the single oceanic plagioclase-bearing cumulative complex buried to eclogite-facies conditions during subduction (Pilitsyna et al., in press).

2.4. Dismembered ophiolites and unmetamorphosed granitoids

In the NE of the Anrakhai block metamorphic formations of the KC have been overthrust by fragments of dismembered ophiolites, represented by serpentinites with bodies of banded, strongly deformed amphibole-bearing gabbroids. On the analogy with the Dzhalair-Naiman zone (considered above), the ophiolites are thought to be of Cambrian age. The chemical compositions of the gabbroids correspond to suprasubductional setting of their formation (Pilitsyna et al., in press). In many cases contacts between the ophiolites and the metamorphic rocks of the KC are marked by orange-colored listvenite-like metasomatic lithologies, consisting of carbonate, feldspar and quartz (Fig. 2, d). These may have been formed during tectonic juxtaposition of the ophiolites and metasedimentary complexes of the KC.

From the NE, the KC and the ophiolites are bounded by an unmetamorphosed body of granodiorite-granite with an estimated protolith age of 509 ± 3 Ma (SHRIMP II), corresponding to Middle Cambrian. The chemical compositions of the granitoids indicate suprasubductional derivation within an ensialic island arc (Alexeiev et al., 2011).

3. Results

As mentioned earlier, the high-pressure ultramafic and mafic lithologies of the KC have been studied in detail (Pilitsyna et al., 2018a, 2018b). On the other hand, information about chemical compositions, P-T-t paths and sources of the country-rocks enclosing the high-pressure ultramafic/mafic formations is virtually absent. Furthermore, obtained detrital zircon ages for the country-rocks provided by Alexeiev et al. (2011) require additional confirmation with better grain number statistics. Reliable data about the chemical compositions, protolith ages and sources of widespread felsic gneissic complexes of the AC are also lacking. Hence, detailed studies of petrography, whole-rock chemical compositions (including whole-rock isotopic data) and mineral chemistry as well as geochronological zircon age determinations of the principal rock types of the AC and KC in the Zheltau terrane have been conducted.

The analytical technique and standards used for the whole-rock and mineral chemistry studies, zircon age determinations and Sm—Nd whole-rock isotopic systematics measurements are provided in Appendices A, C.

3.1. Petrography of the main rock types

3.1.1. Studied rock types of the AC

Muscovite-chlorite orthogneisses are the prevailing variety of the studied area and comprise approximately 60–70% of the AC (Fig. 2). The rocks show monotonously similar petrography throughout and are characterized by medium-grained texture and gneissic structure, where plagioclase (Pl), quartz (Qz) and less K-feldspar (Kfs) with chlorite (Chl) form bands following the lineation (Fig. 3, a). Pl is the predominant feldspar relative to Kfs in these rocks and is frequently replaced by sericite (Ser) to various extents. Pl forms tabular or anhedral crystals up to 1.2–1.5 mm in size, often with well-developed twinning bands. Kfs forms anhedral roundish crystals with sizes varying from 0.2 to 0.8 mm, in some cases with poor grating structure preserved. Quartz

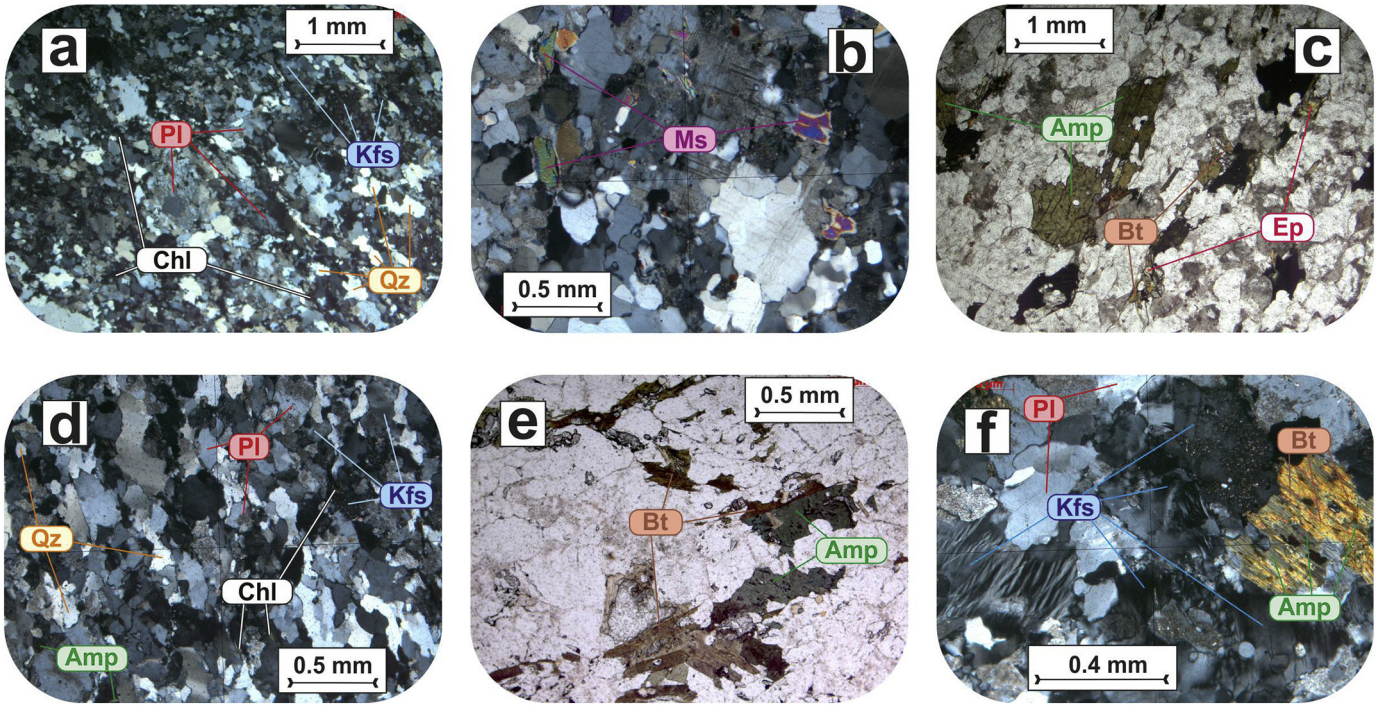

Fig. 3. Photomicrographs of minerals and microtextures of the AC rock types (a, b - muscovite-chlorite orthogneisses; c – f - amphibole-biotite orthogneisses): a) oriented microtexture, composed of plagioclase, quartz, K-feldspar, minor chlorite (crossed nicols); b) flakes of muscovite in the matrix (crossed nicols); c) general microtexture of medium-grained amphibole-biotite orthogneiss (plane light); d) general microtexture of medium-to-fine-grained variety of Amp-Bt orthogneiss; e) flakes of biotite in amphibole-biotite orthogneiss (plane light); f) crystals of K-feldspar with grating structures. Qz – quartz; Pl – plagioclase; Kfs – K-feldspar; Chl – chlorite; Amp – amphibole; Bt – biotite; Ep – epidote.

is characterized by typical clouded extinction; its sizes vary considerably, but normally do not exceed 1 mm. Micas are poorly developed in the rocks; in some cases, muscovite (Ms) is predominant (Fig. 3, b), whereas green Chl (formed evidently after biotite (Bt)) shows subordinate development. However, in most cases, chlorite with relics of brown biotite is more common for the rocks. Both muscovite and chlorite with relics of Bt form flakes ranging from 0.05 to 0.7 mm in size. The rocks contain a number of rounded grains of zircon (~ 0.1 mm) and apatite (up to 0.2 mm) as accessories.

Amphibole-biotite orthogneisses form a narrow tectonic slice up to 1 km wide among the above-described Ms-Chl orthogneisses (Fig. 2). In the field, the rocks are characterized by a reddish colour related to considerable contents of pelitized Kfs, which is prevalent in feldspar relative to Pl. Moreover, the amphibole-biotite orthogneisses include predominant coarse-to-medium-grained varieties with abundant well-developed amphibole (Amp), Bt and even garnet (Grt) (Fig. 3, c) and medium-to-fine-grained orthogneisses with minor Amp and Bt (which may have been considered as associated additional intrusions (Fig. 3, d)). Both varieties are characterized by gneissic textures, where main minerals generally form bands that are oriented in accordance with lineation. Amphiboles represent both euhedral and anhedral crystals of brightly green colour with sizes varying from 0.2 mm to 1.5 mm and coarser (Figs. 3, c, e). In addition, chlorite and later amphibole (actinolite) are developed in the cracks of the amphibole crystals. In many cases, biotite replaces Amp or forms separated brown flakes up to 1 mm in size (Fig. 3, e). Kfs is characterized by wide development, forming euhedral crystals of 0.2–1 mm in size, and it exhibits prominent grating structures (Fig. 3, f). As mentioned earlier, Kfs is intensively pelitized. Plagioclase and quartz are represented by euhedral and often roundish crystals up to 1–1.2 mm in size; plagioclase is normally slightly replaced by Ser. Two colourless roundish grains of garnet were identified in the Amp-Bt orthogneisses, the sizes of which are ~ 0.1 mm. Furthermore, yellowish crystals of epidote are sporadically developed in the rock matrix. Zircon, titanite, apatite and minor carbonate are also present in the rocks.

3.1.2. Studied rock types of the KC

Garnet-mica schists (garnet-kyanite-phengite-K-feldspar-bearing paragneisses) are the main variety among the KC rock types. The rocks are overwhelmingly strongly retrogressed, but minerals indicating high-pressure origin kyanite (Ky), phengite (Ph), and K-feldspar (Kfs) (e.g., O'Brien and Rötzler (2003); Kotková (2007)) are normally preserved as inclusions within marginal parts of garnet or in the matrix. The common minerals of the observed rock type are garnet, which form roundish euhedral pinkish grains of 0.5–1.5-2 mm in size, brown biotite and colourless muscovite representing subanhedral flakes of ~ 0.3–0.7 mm in size, and plagioclase and quartz, which are characterized by clouded extinction and sizes that can exceed 1.5 mm (Figs. 4, a, b). These minerals form ribbons and bands that follow the lineation and foliation. As mentioned earlier, relics of Ky and Ph are normally enclosed within garnet grains, however in some cases relics of Kfs, Ph and Ky are also occasionally developed in the groundmass (Figs. 4, b – f). Tourmaline (Tur) and rutile (Rt) (often replaced by titanite) are also present in the studied rocks. Dark-green tourmaline forms anhedral grains (up to 0.3 mm in size) within the matrix (Supplementary Fig. S4), whereas rutiles are developed both as inclusions in garnet grains and in the groundmass (Figs. 4, f). Rounded grains of zircon, monazite, apatite (0.1–0.3 mm in size) and minor epidote with chlorite, replacing biotite, are widespread in the garnet-mica schists. Notably, apatite grains contain exsolved inclusions of monazite. Thus, in accordance with the mineral compositions the observed garnet-mica schists are thought to be considered as high-pressure granulites (O'Brien and Rötzler, 2003), which were evidently undergone by pervasive retrogressive alterations.

Notably, among the garnet-mica schists with relics of minerals of high-pressure origin at least two types of rocks might be distinguished in accordance with the petrography. The first type (mica-rich sample AH 1470) is characterized by abundance of biotite and white mica, replacing garnet (Fig. 4, a, b); the sizes of garnet do not exceed 1 mm, and Ky with Ph are solely present as relict inclusions in the marginal parts of the garnet. The second type of the rocks (garnet-rich sample Z 12375) possess considerably coarser microtextures, where sizes of the

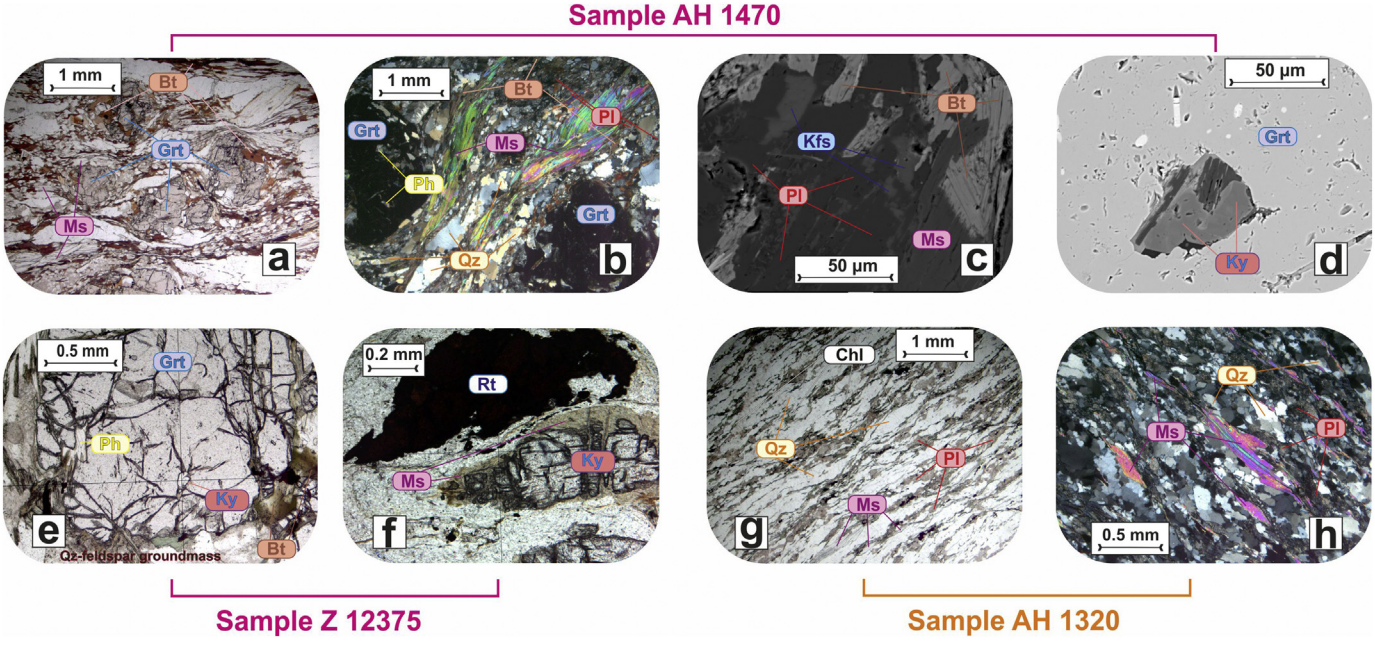

Fig. 4. Photomicrographs of minerals and microtextures of the KC rock types (a – f - garnet-mica schists; g, h - muscovite-chlorite schists): a) foliated microtexture, composed of garnet, micas (biotite, muscovite), feldspar and quartz (plane light); b) porphyroblasts of garnet with inclusions of phengite (crossed nicols); c) back-scattered electron (BSE) image of relics of K-feldspar in the groundmass; d) BSE image of kyanite, enclosed in garnet; e) porphyroblast of garnet with inclusion of kyanite; f) rutile and kyanite in the matrix (plane light); g) general foliated microtexture of muscovite-chlorite schist (plane light); h) flakes of muscovite in the groundmass (crossed nicols). Qz – quartz; Pl – plagioclase; Kfs – K-feldspar; Chl – chlorite; Grt – garnet; Bt – biotite; Ms – muscovite; Ph – phengite; Ky – kyanite; Tur – tourmaline.

garnets vary in the range of 1–1.5 mm and more, and kyanite with phengite are present in the groundmass and enclosed in the mantle-to-marginal parts of the garnets (Fig. 4, e, f). Moreover, biotite or muscovite are poorly developed in the rock-type.

Muscovite-chlorite schists are characterized by fine-to-medium grained textures, where main minerals (muscovite, chlorite (formed after biotite), plagioclase and quartz) possess oriented structure following the foliation (Fig. 4, g). The rocks do not contain minerals of high-pressure origin or garnet and are spatially attributed to amphibolites, marbles and metacherts of low metamorphic grade (Fig. 2). Quartz is a prevailing mineral in the Ms-Chl schists, which is commonly characterized by clouded extinction; the sizes of the quartz grains range from 0.05 to 1 mm and coarser. Plagioclase is normally sericitized and forms anhedral crystals of 0.5–0.7 mm in size. Muscovite is represented by coarse flakes up to 1–1.2 mm long with prominent cleavage (Fig. 4, h), whereas green chlorite, in some cases preserving relics of biotite, forms anhedral laths with sizes of <0.5 mm. Minor carbonate and magnetite are present. A number of rounded grains of zircon and apatite were also identified.

3.2. Whole-rock and mineral chemistry

3.2.1. Whole-rock major and trace element geochemistry of the principal rock types of the AC and KC

The chemical compositions of the observed rock types are provided in Table 2. The samples were selected from well-exposed parts of the studied complexes to avoid the influences of impurities from adjacent lithologies. However, the sampling of garnet-mica and muscovite-chlorite schists was accompanied by inevitable difficulties related to the materials' structures; hence, few results of whole-rock geochemistry of the KC rock types are present.

3.2.1.1. Muscovite-chlorite and amphibole-biotite orthogneisses of the AC. In accordance with the Ab-An-Or ternary diagram, both muscovite-chlorite and amphibole-biotite orthogneisses correspond to granites or in some cases to trondhjemites (Fig. 5, a), and both rock types demonstrate wide ranges of SiO_2 contents (68.3–76.17 wt% and 64.38–75.85 wt%, respectively) (Table 2). Furthermore, with increased SiO_2, the alkaline conditions of the Ms-Chl and Amp-Bt orthogneisses gradually decrease from alkali-calcic to calcic-alkalic and calcic series (the modified alkali-lime indexes (MALI) are in the ranges of 3.09–7.36 and 4.85–8.73, respectively) (Fig. 5, b; Table 2). Both rock types also display wide ranges of K_2O/Na_2O ratios (0.52–1.18 and 0.23–1.82, respectively) (Table 2). The Ms-Chl orthogneisses generally fall into the fields of the peraluminous (ASI = 1.1–1.25) series, whereas the Amp-Bt orthogneisses mostly correspond to metaluminous (ASI = 0.83–0.98) or less commonly to peraluminous (ASI = 1.02, 1.11) series (Fig. 5, c). It must be noted that the Ms-Chl orthogneisses generally possess lower ratios of $FeO_{tot}/(FeO_{tot} + MgO)$ in comparison to the Amp-Bt orthogneisses (0.57–0.88 versus 0.69–0.93) (Fig. 5, d; Table 2).

The muscovite-chlorite and amphibole-biotite orthogneisses display enrichment in LREE relative to HREE ($(La/Yb)_n$ ranges from 5 to 14 and 9–15, respectively) (Fig. 6, A). On the chondrite-normalized plot, the amphibole-biotite orthogneisses are characterized by a smooth negative Eu anomaly (Eu/Eu^* = 0.48–0.74). The muscovite-chlorite orthogneisses are also slightly depleted in Eu (Eu/Eu^* = 0.52–0.81), but they tend to show lower concentrations of HREE in comparison to the amphibole-biotite orthogneisses (Fig. 6, A). On the primitive-mantle normalized diagram (Fig. 6, B), both rock types are generally enriched in LILE (with the exception of Sr) and show depletion in Nb, P, and Ti. However, the amphibole-biotite orthogneisses are more enriched in Zr (142–623 ppm), Nb (24–61 ppm), Y (35–98 ppm) and P (170–737 ppm) in comparison to the muscovite-chlorite orthogneisses, with lower concentrations of these elements (Zr = 118–303 ppm; Nb = 10–27 ppm; Y = 23–34 ppm; P = 175–611 ppm).

On the 'Rb vs. Y+Nb' diagram (after Pearce et al., 1984), the amphibole-biotite orthogneisses fall into the within-plate granite field, whereas the muscovite-chlorite orthogneisses fall near the boundary between within-plate and arc-derived granites (Fig. 5, e). On the diagrams after Whalen et al. (1987), both rock types are inclined to have been attributed to the A-type granite field, with the exception of granites with SiO_2 > 70 wt%, corresponding to I-, S-, and M-type granite fields (Figs. 5, f, g, h). On the 'Nb-Y-Ce' diagram (Eby, 1992), the studied rocks fall near the boundary of anorogenic granites derived from a continental crust (A1-type) or mafic source (A2-type) (Fig. 5, i).

3.2.1.2. Garnet-mica and muscovite-chlorite schists of the KC. The studied schists are characterized by high contents of SiO_2 (71.83–77.24 wt%) and moderate contents of Al_2O_3 (8.97–13.16 wt%) (Table 2). In accordance with the '$\log(FeO_{tot}/K_2O)$ vs. $\log(SiO_2/Al_2O_3)$' diagram (Herron, 1988), the garnet-mica and muscovite-chlorite schists correspond to wacke and litharenites, respectively (Supplementary Fig. S1). The schists show values of chemical index of alteration (CIA = 61–69) that are not very high in comparison to Post-Archean Australian Shale (PAAS) (with CIA = 70), indicating the negligible extent of weathering of their protolith (Nesbitt and Young, 1982, 1984; Taylor and McLennan, 1985).

On the chondrite-, PAAS-, and primitive mantle-normalized diagrams (Figs. 6, C, D, E), the garnet-mica and muscovite-chlorite schists show generally similar patterns of trace element distributions, but the garnet-mica schist is considerably more enriched in LREE, MREE and LILE. Fractionated REE spectra ($(La/Yb)_n$ = 7–15) and negative Eu anomaly (Eu/Eu^* = 0.54–0.62) may reflect the presence of felsic igneous complexes in the source.

3.2.2. Mineral chemistry of the principal rock types of the AC and KC

The muscovite-chlorite orthogneisses of the AC and muscovite-chlorite schists of the KC possess quite monotonous petrographies, and their mineral chemistry is not sufficiently representative to draw reliable conclusions about their P-T evolutions and minerogenesis reactions. On the other hand, the amphibole-biotite orthogneisses of the AC and particularly the garnet-mica schists of the KC are characterized by the presence of metamorphic index minerals; the chemical compositions of the latter varieties are provided in Supplementary tables S1 – S6.

Amphibole is present in the Amp-Bt orthogneisses of the AC and is characterized by perceptible contents of $FeO_{(tot)}$ (26.2–27.04 wt%), TiO_2 (0.95–1.19 wt%), K_2O (1.53–1.99 wt%) and MnO (0.93–1.09 wt%), whereas the MgO contents are low (4.16–4.78 wt%) (Table S1). The amphiboles do not reveal prominent zonation and correspond to potassium-rich hastingsite (Supplementary Fig. S2, a). Occasionally later actinolite (with Si = 7.72 a.p.f.u. and $Mg/(Mg + Fe^{2+})$ = 0.53) is developed in the cracks of hastingsite.

Feldspar is a widespread mineral in both the amphibole-biotite orthogneisses and garnet-mica schists. The plagioclase of the Amp-Bt orthogneisses is albite (X_{ab} varies in the range of 0.91–0.93) (Table S2), whereas in the garnet-mica schists, the compositions of plagioclase change considerably (X_{ab} = 0.68–0.81 in the mica-rich schist AH 1470; X_{ab} = 0.78–0.94 in the garnet-rich schist Z 12375), mostly corresponding to oligoclase-andesine and albite-oligoclase for the samples AH 1470 and Z 12375, respectively (Table S2; Supplementary Fig. S2, b). Potassium feldspar is abundant in the Amp-Bt orthogneisses and corresponds to orthoclase with X_{or} varying from 0.87 to 0.96 (Table S2), whereas in the garnet-mica schists, only relics of K-feldspar (orthoclase-sanidine) with X_{or} = 0.87–0.98 in the matrix are preserved (Table S2; Supplementary Fig. S2, b).

Garnet of the amphibole-biotite orthogneisses of the AC is sporadic and shows high contents of MnO (6.23–7.13 wt%) and FeO (21.66–22.42 wt%) and very low concentrations of MgO (0.1–0.14 wt%) (Table S3; Supplementary Fig. S2, c). The garnets do not reveal zonation and do not contain any inclusions. In the garnet-mica schists a number

Table 2
Selected chemical analyses of the observed rock-types of the AC and KC. Major elements are in wt%, trace elements are in ppm. Mg# = MgO/(MgO + $FeO_{(tot)}$); $FeO_{(tot)} = 0.9Fe_2O_3 + FeO$; n.d. is 'not determined'; LOI is 'loss on ignition'; MALI is 'modified alkali-lime index' = $Na_2O + K_2O$-CaO (Frost et al., 2001); ASI is 'aluminum saturation index' = Al/(Ca - 1.67P + Na + K) (Frost and Frost, 2011); CIA is 'chemical index of alteration' = $Al_2O_3/(Al_2O_3 + CaO + Na_2O + K_2O)$*100 (Nesbitt and Young, 1982, 1984; Taylor and McLennan, 1985).

Sample	Neoproterozoic muscovite-chlorite orthogneisses					Palaeoproterozoic amphibole-biotite orthogneisses									Garnet-mica schists		Muscovite-chlorite schist
	TS 1185	TS 1187/1	TS 1187/2	P 10092	P 10091/1	Z 12371	Z 12371/2	TS 1191	TS 1191/1	TS 1193/1	AH 1316	AH 1317/2	AH 1514	AHP 1515	AH 1470	Z 12375	AH 1320
SiO_2	68.30	74.26	76.17	74.45	75.47	68.33	75.85	75.76	64.51	64.38	70.36	74.46	71.54	70.88	71.83	74.79	77.24
TiO_2	0.37	0.28	0.45	0.43	0.18	0.68	0.24	0.27	0.70	0.95	0.48	0.25	0.50	0.56	0.63	0.88	0.66
Al_2O_3	16.48	14.13	9.45	13.00	13.80	12.67	12.62	11.85	16.94	15.17	12.25	11.97	12.27	12.57	13.16	10.10	8.97
FeO	0.37	1.49	1.93	1.37	0.28	2.16	0.63	1.44	3.36	4.45	1.94	2.14	1.63	2.17	3.57	0.70	2.25
Fe_2O_3	2.06	0.24	0.97	1.38	1.16	4.23	0.45	0.14	1.68	1.07	2.80	0.78	2.82	2.59	1.02	4.91	1.25
MnO	0.05	0.02	0.04	0.06	0.04	0.12	0.04	0.05	0.01	0.05	0.11	0.06	0.09	0.06	0.07	0.10	0.06
MgO	1.65	0.41	1.78	0.59	0.18	0.48	0.22	0.45	2.24	1.57	0.57	0.28	0.36	0.79	2.11	1.81	1.74
CaO	2.02	0.98	2.25	1.51	0.56	1.72	0.41	0.88	2.38	2.24	2.22	1.32	2.03	1.48	1.36	1.33	1.48
K_2O	2.69	3.01	2.89	2.93	3.96	4.95	5.90	5.33	1.33	5.12	5.12	4.92	4.35	5.02	3.06	2.63	2.10
Na_2O	5.16	4.34	2.45	2.78	3.96	3.55	3.24	3.31	5.90	3.88	3.26	3.37	3.89	2.95	1.39	1.05	2.08
P_2O_5	0.05	0.04	0.14	0.05	0.03	0.18	0.04	0.06	0.13	0.29	0.17	0.10	0.15	0.14	0.16	0.20	0.19
LOI	0.78	0.76	1.37	1.30	0.34	0.68	0.31	0.45	0.63	0.72	0.40	0.11	0.20	0.56	1.39	0.96	1.86
Total	99.98	99.96	99.89	99.84	99.96	99.75	99.95	99.99	99.81	99.89	99.68	99.76	99.83	99.77	99.76	99.46	99.86
$\sum K_2O + Na_2O$	7.85	7.35	5.34	5.71	7.92	8.50	9.14	8.64	7.23	9.00	8.38	8.29	8.24	7.97	4.46	3.68	4.18
FeO_{tot}	2.22	1.71	2.80	2.61	1.32	5.97	1.04	1.57	4.87	5.41	4.46	2.84	4.17	4.50	4.49	5.12	3.38
MALI	5.83	6.37	3.09	4.20	7.36	6.78	8.73	7.76	4.85	6.76	6.17	6.97	6.21	6.49			
ASI	1.10	1.16	0.85	1.25	1.17	0.90	1.02	0.93	1.11	0.97	0.83	0.91	0.84	0.98			
Fetot/(Fe_{tot} + Mg)	0.57	0.81	0.61	0.82	0.88	0.93	0.82	0.78	0.69	0.78	0.89	0.91	0.92	0.85	0.68	0.74	0.66
K_2O/Na_2O	0.52	0.69	1.18	1.05	1.00	1.39	1.82	1.61	0.23	1.32	1.57	1.46	1.12	1.70	2.20	2.50	1.01
CIA															69.34	66.84	61.32
Li	17.9	4.2	10.4	–	–	4.8	2.1	3.5	12.4	4.6	n.d.	n.d.	1.8	3.4	n.d.	–	n.d.
Be	2.6	1.9	2.0	–	–	3.8	3.0	1.9	2.5	2.6	n.d.	n.d.	3.9	3.1	1.8	–	n.d.
Sc	10.9	2.2	5.7	–	–	9.0	2.8	4.0	6.4	11.0	n.d.	n.d.	7.3	6.8	14.0	–	n.d.
V	37.2	8.8	25.0	–	–	14.8	7.1	14.7	43.8	31.3	10.9	5.4	13.6	34.9	78.5	–	56.5
Cr	25.1	11.2	24.2	–	–	9.1	11.8	4.8	19.7	1.3	18.0	28.8	10.8	2.8	82.0	–	56.4
Co	6.7	0.8	4.8	–	–	4.7	0.8	0.9	3.0	9.1	3.6	1.9	4.6	5.5	13.0	–	7.0
Ni	34.6	6.2	13.8	–	–	10.1	17.9	4.3	1.2	2.4	9.7	16.2	7.9	3.2	38.2	–	21.3
Cu	7.7	4.5	10.9	–	–	8.3	3.0	13.1	3.6	10.1	9.9	7.7	7.7	4.7	23.5	–	9.0
Zn	56.3	28.2	33.7	–	–	144.0	34.0	43.1	34.0	60.4	84.0	68.7	97.9	56.2	68.6	–	33.9
Ga	24.7	10.7	12.4	–	–	18.9	12.3	14.1	16.2	20.5	19.2	17.4	19.1	16.7	18.1	–	8.5
Rb	73.4	61.8	83.6	–	–	150.0	198.0	130.5	30.5	125.7	107.0	115.0	111.6	123.4	140.0	–	59.5
Sr	900.0	141.5	139.4	–	–	178.0	82.3	92.9	188.2	95.7	130.0	119.0	150.6	261.7	135.0	–	95.5
Y	34.2	22.8	24.4	–	–	94.2	35.4	37.6	64.6	60.1	79.9	44.2	90.4	98.1	32.6	–	22.5
Zr	259.0	118.5	302.7	–	–	562.0	161.0	142.4	493.2	532.4	588.0	623.0	325.4	252.7	69.5	–	269.0
Nb	26.8	18.7	10.1	–	–	49.0	24.8	17.8	33.9	28.0	39.7	25.5	60.7	52.3	8.2	–	7.7
Mo	1.3	0.3	0.4	–	–	1.1	1.4	0.2	0.2	0.1	0.7	0.6	1.4	1.1	0.7	–	0.0
Cs	2.9	0.6	0.7	–	–	0.4	0.4	0.3	0.4	0.3	0.8	0.4	0.3	0.4	5.5	–	0.6
Ba	1260.0	694.7	579.6	–	–	1422.0	1338.0	827.5	438.8	660.3	1230.0	1240.0	1240.1	1718.0	601.0	–	282.0
La	69.8	57.4	37.3	–	–	95.3	55.3	41.8	78.3	74.2	90.3	99.4	92.4	102.7	57.8	–	27.5
Ce	131.0	102.3	79.1	–	–	200.0	111.0	87.2	166.2	154.6	166.0	172.0	195.2	216.6	121.0	–	51.0
Pr	14.2	9.9	8.2	–	–	24.0	11.6	9.0	19.1	17.2	20.9	18.4	23.0	24.7	11.5	–	5.8
Nd	50.4	33.0	30.4	–	–	87.5	41.8	33.4	74.3	65.6	77.3	67.9	88.3	94.4	46.3	–	21.2
Sm	8.6	5.6	5.7	–	–	17.8	7.7	6.6	15.1	13.2	14.7	11.8	17.7	19.3	9.8	–	4.4
Eu	2.1	0.9	0.9	–	–	3.5	1.3	1.0	3.1	2.5	3.4	2.2	3.5	3.2	1.5	–	0.9
Gd	7.3	4.7	5.1	–	–	17.5	6.8	6.6	15.2	12.8	13.8	10.3	17.9	19.6	7.6	–	4.0
Tb	1.1	0.7	0.8	–	–	2.8	1.1	1.1	2.3	2.0	2.2	1.5	2.7	3.0	1.0	–	0.6
Dy	6.2	3.9	4.3	–	–	16.9	6.2	6.9	13.1	11.8	14.2	9.5	15.9	17.3	5.1	–	3.6
Ho	1.2	0.8	0.9	–	–	3.3	1.3	1.5	2.5	2.3	2.8	1.8	3.2	3.5	1.0	–	0.8
Er	3.6	2.4	2.6	–	–	10.1	3.8	4.7	6.7	6.9	9.0	4.9	9.6	10.5	2.3	–	2.4
Tm	0.5	0.4	0.4	–	–	1.4	0.6	0.7	0.9	1.0	1.2	0.7	1.3	1.4	0.4	–	0.3
Yb	3.3	2.5	2.6	–	–	9.3	3.8	5.1	5.6	6.3	7.4	4.6	8.8	9.1	2.5	–	2.4

Lu	0.5	0.4	0.4	–	–	1.3	0.5	0.8	0.8	0.9	1.2	0.7	1.2	1.2	0.3	–	0.3	
Hf	6.2	3.4	7.8	–	–	14.2	5.6	4.5	11.9	12.2	15.7	15.3	9.5	7.6	1.9	–	6.8	
Ta	1.6	1.8	1.0	–	–	2.9	1.7	1.5	2.6	1.6	2.4	1.3	3.1	3.6	0.7	–	0.7	
W	0.4	0.8	0.3	–	–	0.1	0.2	0.1	0.2	0.2	n.d.	n.d.	0.2	0.3	1.1	–	1.0	
Tl	0.6	0.3	0.4	–	–	0.8	1.0	0.8	0.2	0.7	n.d.	n.d.	0.6	0.7	n.d.	–	n.d.	
Pb	39.0	14.5	8.1	–	–	27.8	12.7	25.0	11.0	152.4	13.2	18.9	20.0	29.9	23.0	–	9.1	
Bi	0.1	0.04	0.2	–	–	0.02	0.04	0.03	0.01	0.03	n.d.	n.d.	n.d.	n.d.	n.d.	–	n.d.	
Th	15.8	19.4	15.2	–	–	17.8	14.3	13.2	14.4	17.4	15.0	15.3	13.3	17.3	21.0	–	11.6	
U	2.6	2.0	1.5	–	–	2.5	1.7	2.0	2.5	2.5	2.0	0.9	1.3	1.1	3.0	–	1.4	

of garnet grains displays prominent chemical zonation. On the basis of the element distributions, at least two varieties of garnet have been identified. Garnet I (Fig. 7, A) is characterized by preserved "prograde" chemical zonation, reflected by bell-shaped profile of MnO (from 2.42 wt% in the core to 0.18 wt% in the rim) and MgO with CaO increasing in the same direction (from 1.08 to 3.3 wt% and from 6.61 to 10.18 wt%, respectively) (Table S3; Supplementary Fig. S2, c). Garnet II (Fig. 7, B) exhibits relatively chemically homogenous cores, in particularly with respect to MnO contents. At the same time mantle parts and rims of the Garnet II demonstrate decrease of FeO and CaO (from 29.64 to 23.18 wt% and from 5.30 to 3.84 wt%, respectively), compensated by MgO growth in the same direction (from 5.22 to 10.23 wt%) (Table S3; Supplementary Fig. S2, c). Notably, CaO distribution in the Garnet II evidently reflects two stages, where the first stage is expressed in gentle CaO increasing from core to mantle parts, and the second stage is characterized by abrupt dropping in calcium contents (Fig. 7, B). The first type of zonation (Garnet I) could be considered as growth zoning, whereas the second type (Garnet II) generally represents an example of diffusion zoning (Spear, 1993).

As mentioned earlier, the garnets of the schists contain numerous inclusions of micas, kyanite and rutile.

White mica of the garnet-mica schists includes muscovite and phengite. Muscovite has direct boundaries with biotite in the garnet-mica schist AH 1470 and shows notable contents of TiO_2 (0.86–0.91 wt%), Na_2O (X_{Pg} ~ 0.09) and MgO (X_{Phl} ~ 0.08) (Table S4). Most SiO_2 contents exceed 45 wt%. Muscovite from the garnet-rich schist Z 12375 is alternatively characterized by lower contents of MgO (X_{Phl} ~ 0.05–0.07) and higher contents of FeO (X_{Ann} ~ 0.09–0.10) in comparison to the sample AH 1470. Muscovite is poorly developed in the garnet-rich schist Z 12375 and often replaces kyanite in the groundmass (Fig. 4, f; Table S4). Phengite is mainly developed as inclusions in garnet of the garnet-mica schists in the KC and sporadically presented in the groundmass. Ph shows Si (atoms per formula unit (a.p.f.u.)) in the range of 3.28–3.32. In comparison to the above-described muscovite, relics of phengite possess higher MgO contents (X_{Phl} varies from 0.10 to 0.12) (Table S4). Notably, phengite from the garnet-rich schist Z 12375 displays higher contents of FeO (X_{Ann} ~ 0.12–0.14) in comparison to the mica-rich schist AH 1470 (Table S4).

Biotite of the garnet-mica schists of the KC is characterized by high MgO contents (X_{Phl} is approximately 0.4) and moderate FeO contents (X_{Ann} ranges from 0.41–0.44) (Table S4). Frequently, biotite is replaced by chlorite (picnochlorite). In the mica-rich sample AH 1470 biotite adjacent to the garnet rims possesses higher contents of MgO, compared to biotite, bounded by quartz-feldspar aggregates (Supplementary Fig. S3).

Tourmaline is solely widespread in the garnet-mica schists in the KC. Tur is characterized by high contents of Al_2O_3 (28–29 wt%) and MgO (6–7 wt%) and corresponds to magnesio-foitite (Table S5; Supplementary Fig. S4). Tur contains numerous inclusions of quartz. Other indicative minerals of the garnet-mica schists are *rutile* (frequently replaced by titanite) with high contents of ZrO (in the range of 0.10–0.16 wt%) and kyanite, showing a typical balance between Al_2O_3 and SiO_2. However, notable contents of FeO are detected (Tables S5, S6).

3.3. Metamorphism of the principal rock types of the AC and KC

As indicated in Parts 3.1 and 3.2 above, the formations of the Zheltau terrane evidently underwent metamorphic alterations of various grades. However, the characteristics of the appearing metamorphic changes are different for the AC and KC. The methods of thermodynamic modelling and conventional geothermobarometry as well as petrographic and field observations have been used to estimate the approximate P-T paths of the studied rocks of the AC and KC. The incorporated bulk compositions, thermodynamic databases and solution models for P-T pseudosection modelling are provided in Appendix B.

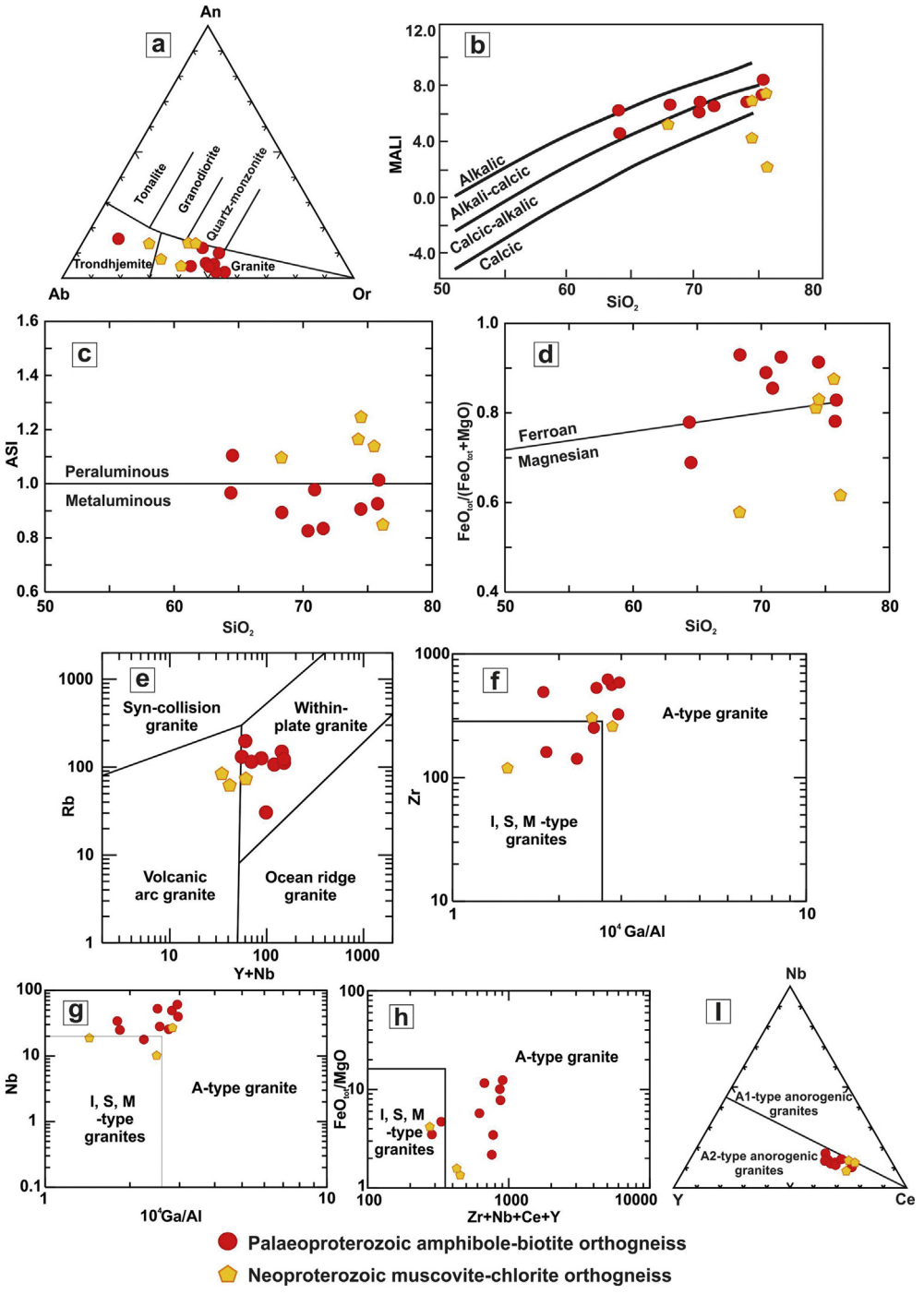

Fig. 5. Variation diagrams (a – d) and tectono-magmatic diagrams (e – i) for muscovite-chlorite and amphibole-biotite orthogneisses: a) Ab-An-Or classification of granitoids (Barker, 1979); b) MALI (modified alkali lime index) vs SiO_2 plot (Frost et al., 2001); c) ASI (aluminum saturation index) vs SiO_2 plot (Frost and Frost, 2011); d) $FeO_{tot}/(FeO_{tot} + MgO)$ vs SiO_2 plot (Frost et al., 2001); e) Rb vs Y + Nb plot (Pearce et al., 1984); f) Zr vs 10^4Ga/Al plot (Whalen et al., 1987); g) Nb vs 10^4Ga/Al (Whalen et al., 1987); h) FeO_{tot}/MgO vs Zr + Nb + Ce + Y (Whalen et al., 1987); i) Nb-Y-Ce ternary plot (Eby, 1992).

3.3.1. Metamorphism of the muscovite-chlorite and amphibole-biotite orthogneisses of the AC

In accordance with the mineral compositions of both types of orthogneisses, metamorphic alterations in the rocks apparently did not exceed the conditions of amphibolite facies. The petrography of the muscovite-chlorite orthogneisses is quite monotonous; nevertheless, taking into account that the rocks contain bodies of amphibolites (Fig. 2) and that biotite is mostly replaced by chlorite, metamorphic alterations of the muscovite-chlorite orthogneisses likely correspond to low-moderate grades (i.e., greenschist – epidote-amphibolite facies). The amphibole-biotite orthogneisses are characterized by a more representative petrography, including garnet, epidote and amphibole, indicating alterations at epidote-amphibolite-facies conditions. It is additionally confirmed by the intersection of compositional isopleths of Grt (X_{Mn} and $X_{Mg/(Fe+Mg)}$), Amp ($Na_{(a.p.f.u.)}$ and $Ca_{(a.p.f.u.)}$) and Pl (X_{an}) in the wide range of pressures (6.5–10 kbar) at T 480–550 °C (Supplementary Fig. S5; Tables S1, S2, S3), corresponding to epidote-amphibolite facies. The amphibole geobarometers of Hammarstrom and Zen (1986), Hollister et al. (1987), Johnson and Rutherford (1989) and Schmidt (1992) applied to amphiboles from the orthogneisses

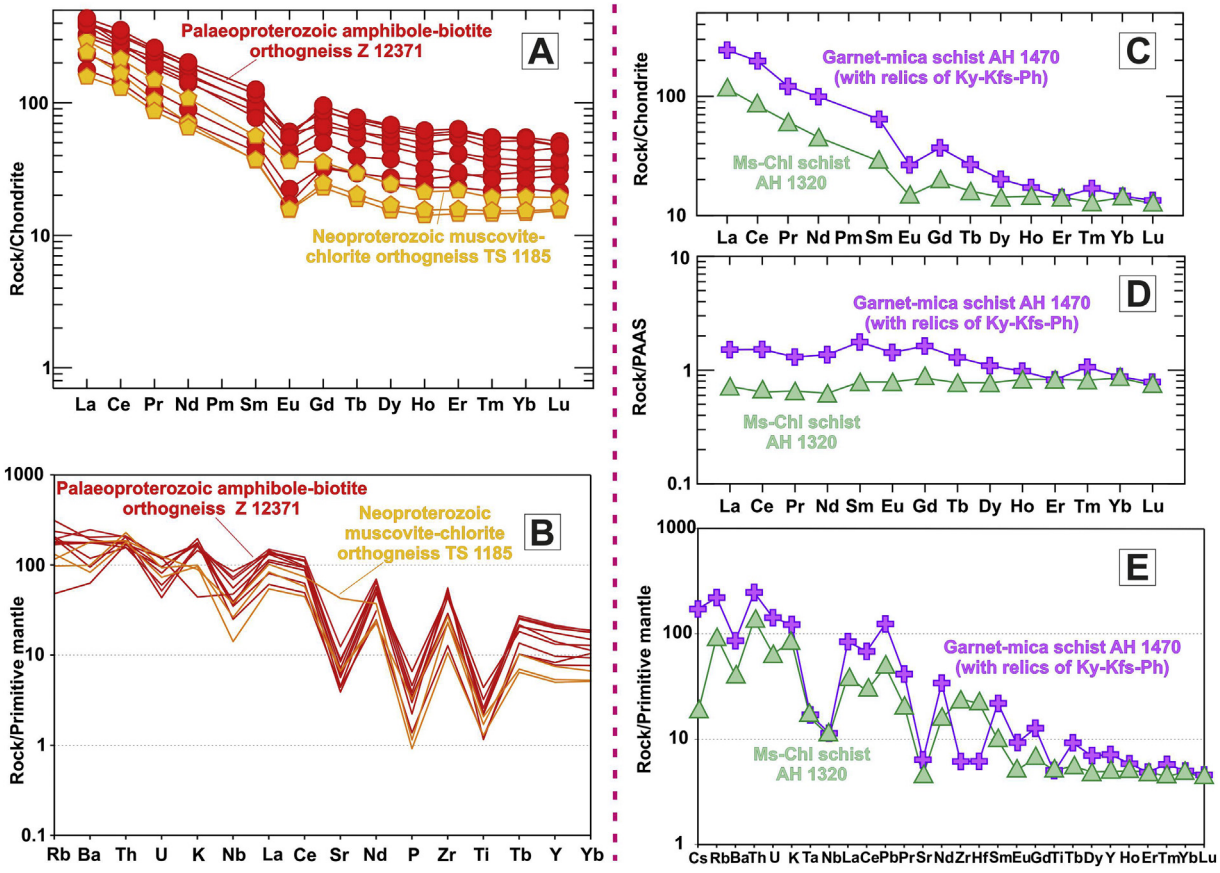

Fig. 6. (A) Chondrite- and (B) primitive mantle- normalized patterns for the muscovite-chlorite and amphibole-biotite orthogneisses. (C) Chondrite-, (D) PAAS- and (E) primitive mantle-normalized patterns for the garnet-mica and muscovite-chlorite schists. Chondrite and primitive mantle values are from Sun and McDonough (1989). PAAS composition is from Taylor and McLennan (1985).

yielded pressures in the close range of 5–7.3 kbar. Formation of actinolite and chlorite, which are sporadically present in the cracks of the amphibole crystals, might have been related to retrogression in the greenschist-facies field.

Notably, the studied orthogneisses of the AC *do not* contain minerals or relics of minerals of high-pressure origin. On the other hand, as indicated in Part 2.1, in the SE of the Anrakhai block (Fig. 2) the rocks of the Anrakhai and Koyandy complexes evidently experienced the high-grade metamorphism with partial melting and subsequent migmatization of the Qz-Fsp-bearing rocks of the complexes. However, thorough studies of the index-minerals in the felsic *metamagmatic* formations of the AC in this part of block have not been conducted so far.

3.3.2. Metamorphism of the garnet-mica and muscovite-chlorite schists of the KC

The garnet-mica schists are the prevalent variety in the KC. Despite strong retrogression, the rocks tend to preserve numerous relics of minerals, indicating their high-pressure derivation and could be classified as strongly altered high-pressure granulites (O'Brien and Rötzler, 2003). Thus, different samples of the garnet-mica schists were selected in the NW, central and SE parts of the complex (Fig. 2); in all cases, the selected rocks contain kyanite and phengite and relics of K-feldspar (Parts 3.1.2 and 3.2.2 above). Moreover, the garnet-mica schists contain pods of eclogites, garnet clinopyroxenites and spinel-bearing ultramafites formed at high-pressure conditions of at least P 14–17 kbar and T 700–800 °C (Pilitsyna et al., 2018a, b).

In accordance with the Parts 3.1.2 and 3.2.2, several grains of garnet of the schists (e.g. mica-rich sample AH 1470) are characterized by a prominent "prograde" zonation from core to rims (Fig. 7, A) (Garnet I). This indicates that metamorphic evolution of the rocks evidently included prograde stages with garnet nucleation (corresponding to the most manganese central parts), the gradual growth of garnet and a following peak of metamorphism, implying a 'clockwise' P-T path for the studied rocks. The observed bell-shaped profile of Mn distribution in the Garnet I is considered to represent a remnant of the growth zoning, preserved to some extent. However, assuming high-grade conditions of the rocks re-equilibration, confirmed by a presence of the index-minerals (Ky, Ph) as inclusions within the garnet mantle-to-rim parts, it is suggested that the garnet zoning must be modified by high-temperature diffusion, which would obscure most features of the earlier growth zoning. Nevertheless, a preservation of the garnet prograde zoning in the high-grade metapelites is not an extraordinary case for the metamorphic complexes, formed in subduction-collisional settings (considered in Part 4.2 below). At the same time, garnets from the sample Z 12375 possess the common features of diffusional zoning in the high-temperature conditions (Fig. 7, B) (Garnet II) with gradual increase of Mg from core to rims, compensated by Fe decrease in the same direction, whereas distribution of Mn is almost "flat". Taking into consideration the observed features of element distributions in the garnets of the samples AH 1470 and Z 12375 together with the mineral assemblages, developed in the indicated rocks, the approximate P-T paths for the prograde, near-peak and retrograde stages in the garnet-mica schists have been described and estimated.

3.3.2.1. Prograde stage of metamorphism. Intersection of the compositional isopleths of the garnet core from the mica-rich sample AH 1470 (Garnet I) covers a wide pressure-temperature range of 5–8 kbar at $T = 520–650$ °C. Notably, the gradual increase of Ca from core to mantle parts, observed from the garnet zoning (Fig. 7; 8, a), is interpreted to have been related to increase of pressure during the garnet growth (Indares and Dunning, 2001; Spear and Kohn, 1996). It is confirmed

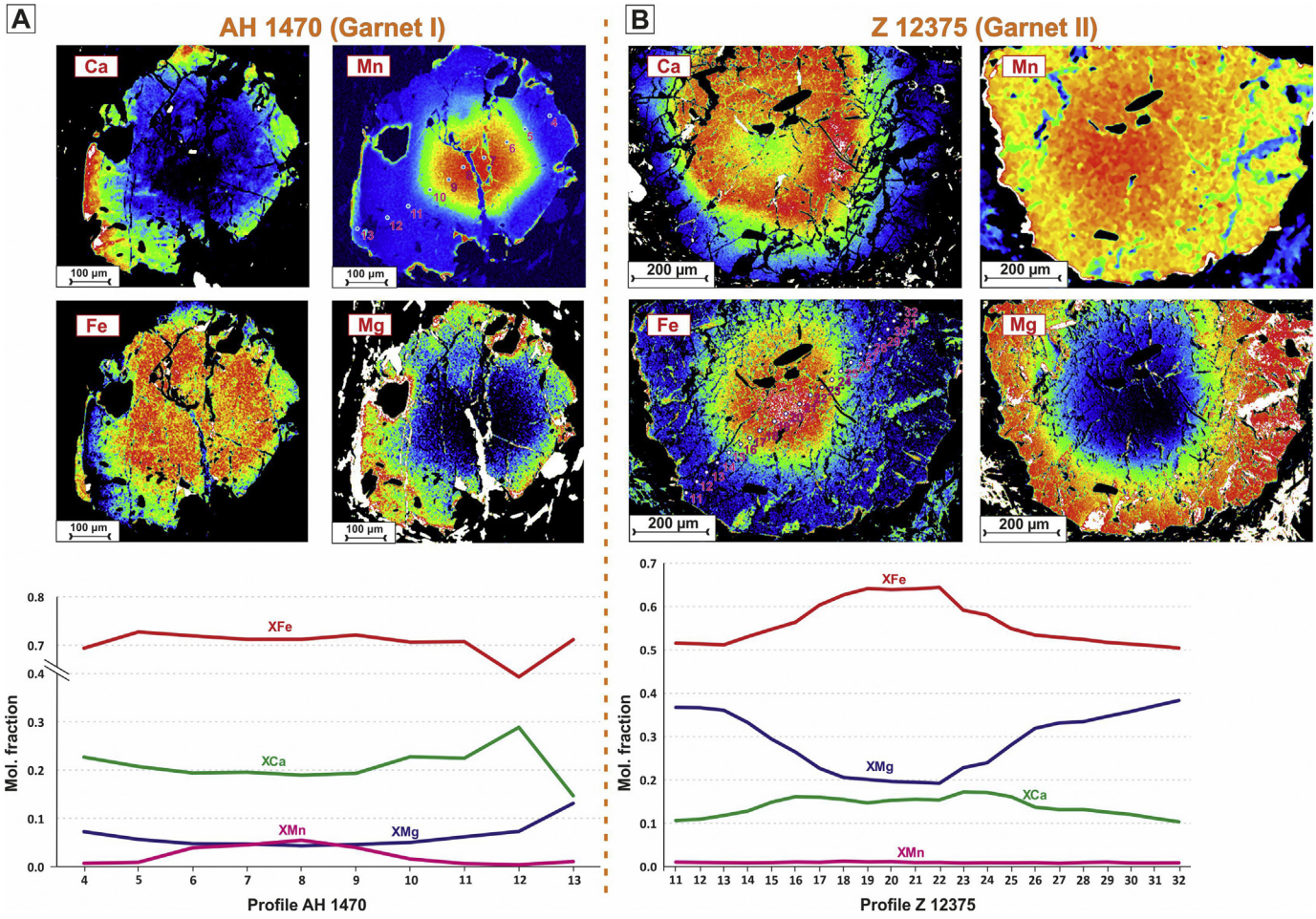

Fig. 7. X-ray element maps (Mg, Mn, Fe, Ca) of garnet from: (A) garnet-mica schist AH 1470 (Garnet I). Points 4–13 on the Mn-map are in accordance with values from Table S3; (B) garnet-mica schist Z 12375 (Garnet II). Points 11–32 on the Fe-map are in accordance with values from Table S3;

by increase of modal proportions of garnet, consistent with Ca growth during the prograde stage, obtained from the modelling (Fig. 8, b). Furthermore, the garnet cores of the sample Z 12375 (Garnet II) are mostly homogenized, driven by diffusion at higher temperatures. Nevertheless, calcium diffusion rates are slow in comparison to Mg, Fe or Mn (Indares, 1995), therefore, preservation of the slight increase of Ca from core to mantle parts of the garnet could be observed (Fig. 7, B). This part of the garnet zoning is evidently consistent with that, described for the sample AH 1470 (Garnet I) and could be interpreted as a relic of the prograde stage zonation. In turn, Ca increase in the studied garnets of the samples AH 1470 and Z 12375 during the prograde evolution of the metapelites might be reflected by a reaction with plagioclase, accompanied by a consumption of anortite, which is also predicted by the modelling (Fig. 8, c).

3.3.2.2. Near-peak stage of metamorphism. With an increase of pressure and temperature during subduction of the studied metapelites, an extensive dehydration melting of micas is expected. In such a scenario, two possible reactions, responsible for the formation of the index-peritectic phases + melt, are suggested: 1) Bt + Ph + Pl + Qz = Grt + Kfs + melt (R1); 2) Ph + Pl + Qz = Grt + Ky + Kfs + melt (R2) (Indares and Dunning, 2001). Thus, an assemblage of Mg-rich garnet with K-feldspar and kyanite might have been considered as corresponding to the near-peak stage of metamorphism.

Despite the presence of a prominent prograde zoning, preserved in some garnet grains in the sample AH 1470 (Fig. 7, A), a pervasive development of biotite, muscovite and Ca-rich plagioclase indicates a drastic re-equilibration of the rock during the retrogression. From here, the observed zoning is evidently incomplete, reduced by a consumption of garnet (as predicted by the modelling on Fig. 8, b). Thus, using of the analyses of garnet from the sample AH 1470 (Table S3) is not appropriate to assess P-T conditions of the near-peak metamorphic stage for the garnet-mica schists.

On the other hand, garnets from the sample Z 12375 (Fig. 7, B) are characterized by the common diffusional zoning (Garnet II) and contain inclusions of phengite or kyanite within the mantle parts or inner rims of the garnet grains (Fig. 4, e), whereas the outer parts are highly magnesian, indicating the retrograde diffusional Fe—Mg exchange with biotite (considered below). In the Fig. 9, A the compositional isopleths of the mantle-to-rim part of garnet (X_{Mn}, X_{Ca}, X_{Fe}, X_{Mg}) intersect with the isopleths of phengite (Si and Mg (a.p.f.u.)) and plagioclase (X_{ab}) (Tables S2, S3, S4) in the multivariate field of P 15–17 kbar and T 750–810 °C, corresponding to high-pressure and moderate-temperature conditions. Notably, the isopleths fall to the boundary of biotite disappearance, indicating a production of Mg-rich part of garnet together with K-feldspar, resulted from the reaction R1, with biotite and partly phengite breakdown. On the other hand, it is shown in Fig. 9, B that kyanite formation commences at higher temperatures (820 °C and more for pressures >12 kbar), which is related to dehydration melting of phengite, driven by the reaction R2. Thus, in accordance to the phase diagram biotite and phengite apparently started to melt concurrently (R1) at temperatures >700 °C, followed by melting of the remaining white mica with production of kyanite (R2) at temperatures >800 °C. This inverse order of melting does not contradict to the experimental studies and is examined in Le Breton and Thomson (1988), Indares and Dunning (2001). Decrease in calcium in the inner parts of the garnet grains, observed from the zoning (Fig. 7, B) together with increase of

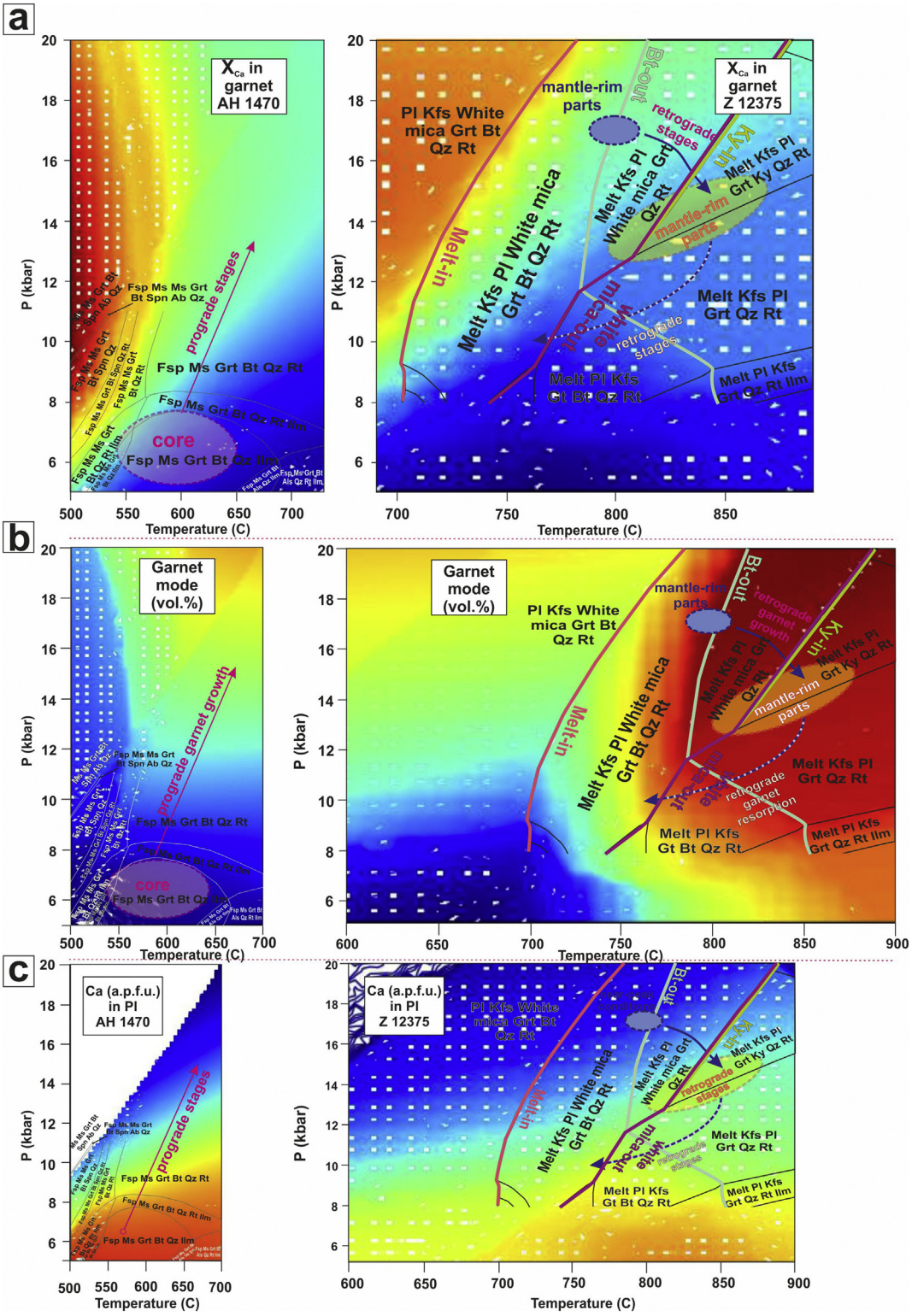

Fig. 8. Compositional isopleths of the garnet-mica schists minerals: a) X_{Ca} distribution in the garnets; b) modal variations (vol%) of garnet in the rocks; c) Ca (a.p.f.u.) distribution in plagioclase. The range from the dark-blue to dark-red colors correspond to the range from MIN to MAX values, respectively. The isopleths were plotted with PyWerami software (Lexa, 2011). Mineral assemblages, wet solidus line and mineral stability fields are from Fig. 9, S6. (For interpretation of the references to colour in this figure legend, the reader is referred to the web version of this article.)

anortite in the associated plagioclase (Supplementary Fig. S3, at the bottom) indicate a reaction of garnet with kyanite (GASP; Ganguly and Saxena (1984)) during the post-peak decompression. In this case insignificant temperature growth might be related to melting propagation in response to an onset of decompression. Notably, growth of Mg-rich garnet at this stage evidently continued during some period of decompression, which is confirmed by the modelling (Fig. 8, b). However, the following extensive growth of retrograde biotite and muscovite, related

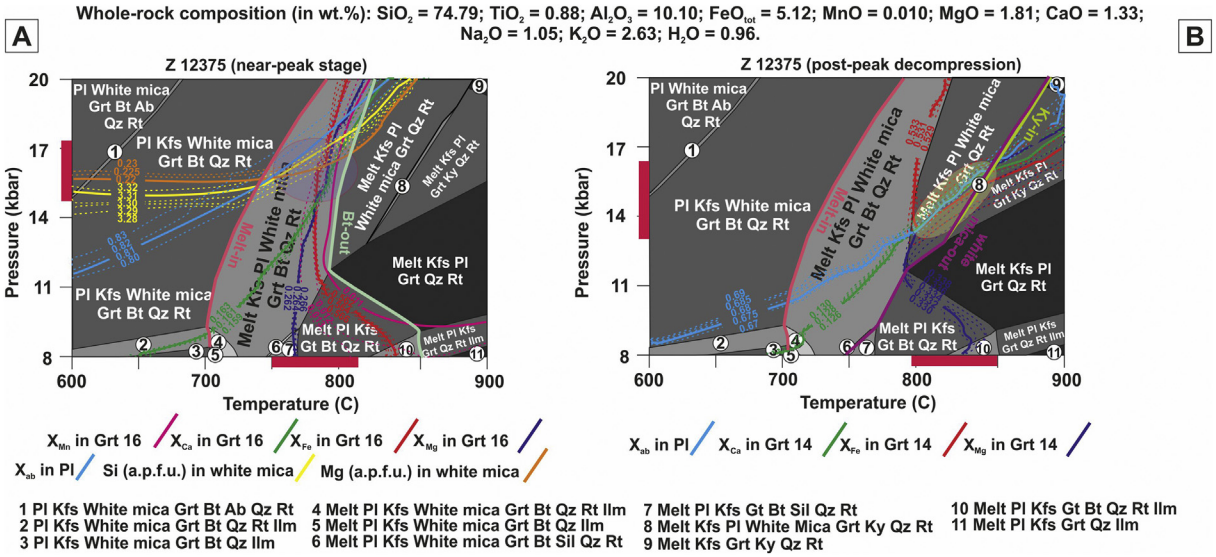

Fig. 9. P-T pseudosections for CFTiMMnNKASH system based upon the measured whole-rock composition for (A) near-peak stage and (B) post-peak decompression stage (garnet-mica schist Z 12375). The details of recalculations and solution models are given in section 3.3.2 and Appendix B. Colored lines are compositional isopleths for: (A) X_{Mn}, X_{Ca}, X_{Fe}, X_{Mg} in Grt 16 (Table S3), X_{ab} in Pl and Si, Mg (a.p.f.u.) in Ph (Tables S2, S4); (B) X_{Ca}, X_{Fe}, X_{Mg} in Grt 14 (Table S3), X_{ab} in Pl (Table S2).

to a fluid release during the melt crystallization, apparently led to resorption of garnet.

An intersection of the compositional isopleths from the inner-rim part of garnet (X_{Ca}, X_{Fe}, X_{Mg}) with plagioclase (X_{ab}) isopleths (Tables S2, S3) corresponds to a P-T range of P 13–16 kbar and T 800–850 °C (Fig. 9, B). The conducted conventional geothermobarometry with the use of Zr-in-Rutile thermometry (Watson et al., 2006) and grossular-aluminosilicate-plagioclase-quartz (GASP) barometry (Ganguly and Saxena, 1984; Koziol and Newton, 1989) showed values in the range of P 16–18 kbar and T 720–830 °C (Table S6), which are interpreted as a near-metamorphic peak. The obtained estimates are consistent with those resulting from thermodynamic modelling.

3.3.2.3. Retrograde stage of metamorphism. Formation of the Mg-rich outer-rim parts of garnet in the studied schists is related to diffusional Fe—Mg exchange with the retrograde biotite (Supplementary Fig. S3), where biotite, adjacent to the garnet rims is notably more enriched in Mg, compared to biotite from the Qz-feldspar aggregates. Using of the Grt – Bt geothermometry (after Perchuk and Lavrent'eva (1983)) showed the temperature range of 580–620 °C, which is consistent to the complete melt crystallization and pervasive development of the new-formed retrograde micas with a concurrent garnet resorption. Moreover, a significant increase of anortite component in the associated plagioclase, compensated by Ca decrease in the garnet rims (Supplementary Fig. S2, b; S3, below), as well as kyanite replacement by muscovite, also indicate the decompression stage at moderate-low P-T conditions (Indares, 1995).

Alternatively, the muscovite-chlorite schists possess subordinate distribution within the KC and are spatially attributed to metacherts, marbles and amphibolites without garnet (Fig. 2). The Ms-Chl schists *do not* contain index minerals of high-pressure origin or even garnet; the main features of the metamorphic alterations of the rocks are the replacement of biotite by chlorite and pervasive foliation. Hence, in accordance with the field observations and petrography, the muscovite-chlorite schists were apparently metamorphosed in the low-moderate grade of epidote-amphibolite facies and not higher.

3.4. Zircon age determinations and Sm—Nd whole-rock isotopic systematics of the principal rock types

3.4.1. Zircon age determinations and Sm—Nd whole-rock isotopic systematics of the muscovite-chlorite and amphibole-biotite orthogneisses of the AC

Zircons from the muscovite-chlorite orthogneiss TS 1185 and amphibole-biotite orthogneiss Z 12371 (Table 2) from the AC have

Table 3
Results of ion-microprobe (SHRIMP II) U-Th-Pb analyses of zircons from the muscovite-chlorite orthogneiss (sample TS 1185).

№ in Fig. 9	$^{206}Pb_c$ %	U, ppm	Th, ppm	$^{206}Pb^*$ppm	$^{232}Th/^{238}U$ ±%		$^{206}Pb/^{238}U$ Age, ±Ma		$^{207}Pb/^{206}Pb$ Age, ±Ma		D, %	$^{207}Pb^*/^{206}Pb^*$ ±%		$^{207}Pb^*/^{235}U$, ±%		$^{206}Pb^*/^{238}U$, ±%		Rho
17.1	0.47	66	105	6.25	1.63	0.50	671	±11	643	±61	-4	0.0611	2.9	0.92	3.3	0.110	1.7	0.5
12.1	0.62	137	227	14	1.72	0.40	726	±11	768	±48	+6	0.0648	2.3	1.07	2.8	0.119	1.7	0.6
15.2	–	128	248	13.8	2.00	0.42	762	±12	809	±35	+6	0.0661	1.7	1.14	2.3	0.126	1.7	0.7
16.1	0.31	158	144	17.2	0.94	0.39	766	±12	752	±38	-2	0.0643	1.8	1.12	2.4	0.126	1.6	0.7
3.1	–	174	356	19	2.11	0.36	769	±12	801	±27	+4	0.0658	1.3	1.15	2.1	0.127	1.6	0.8
5.1	–	478	363	52.3	0.79	0.22	773	±11	825	±17	+7	0.0666	0.8	1.17	1.7	0.127	1.5	0.9
9.1	0.18	393	313	43.3	0.82	0.24	779	±11	809	±21	+4	0.0661	1.0	1.17	1.8	0.128	1.6	0.8
13.1	0.09	770	529	85.5	0.71	0.18	784	±11	778	±14	-1	0.0651	0.7	1.16	1.7	0.129	1.6	0.9
6.1	–	230	500	25.8	2.24	0.32	790	±21	809	±25	+2	0.0661	1.2	1.19	3.0	0.130	2.8	0.9
8.1	0.04	483	714	54.6	1.53	0.22	797	±12	801	±16	+1	0.0658	0.8	1.19	1.7	0.132	1.5	0.9
14.1	0.08	474	397	53.7	0.87	0.22	798	±12	763	±18	-5	0.0646	0.8	1.17	1.8	0.132	1.5	0.9
14.2	0.61	156	213	19.4	1.41	0.37	871	±14	1951	±22	+59	0.1197	1.3	2.39	2.1	0.145	1.7	0.8

Notes: all errors are 1 σ; Pb_c and Pb* indicate the common and radiogenic portions, respectively; common Pb corrected using measured ^{204}Pb.

Table 4
U—Pb isotopic data (ID-TIMS) for zircons from the amphibole-biotite orthogneiss (sample Z 12371).

№	Zircon size (μm) and type of treatment	Weight, (mg)	Concentration, (ppm)			Isotopic ratios corrected for blank and common Pb				Rho	Age, Ma		
			Pb	U	$^{206}Pb/^{204}Pb$[a]	$^{207}Pb/^{206}Pb$	$^{208}Pb/^{206}Pb$	$^{207}Pb/^{235}U$	$^{206}Pb/^{238}U$		$^{207}Pb/^{235}U$	$^{206}Pb/^{238}U$	$^{207}Pb/^{206}Pb$
1	50–80, 30 grains	0.11	21.6	92.0	1202	0.1017 ± 2	0.1887 ± 1	2.8901 ± 63	0.2061 ± 3	0.74	1379 ± 3	1208 ± 2	1656 ± 3
2	85–100, 20 grains	0.50	19.5	75.5	1300	0.1040 ± 1	0.2007 ± 1	3.1865 ± 37	0.2222 ± 2	0.94	1453 ± 2	1293 ± 1	1697 ± 1
3	50–80, CA 2 h.	-*	U/Pb = 30.21		13,035	0.1101 ± 1	0.2062 ± 1	4.4352 ± 52	0.2921 ± 3	0.94	1718 ± 2	1652 ± 2	1801 ± 1
4	85–100, 16 grains A30%	-*	U/Pb = 28.92		570	0.1111 ± 2	0.2204 ± 1	4.5966 ± 102	0.3001 ± 5	0.96	1749 ± 4	1692 ± 3	1817 ± 1

Notes: all errors are 2 σ and refer to last digits of corresponding ratios; CA- zircons after chemical abrasion; A30% - air-abraded zircons, shown percentage - amount of zircon removed during of the air-abrasion; [a] - measured ratio; —* - U/Pb ratios for unweighted grains or residues after the acid treatment were determined using the $^{202}Pb/^{235}U$.

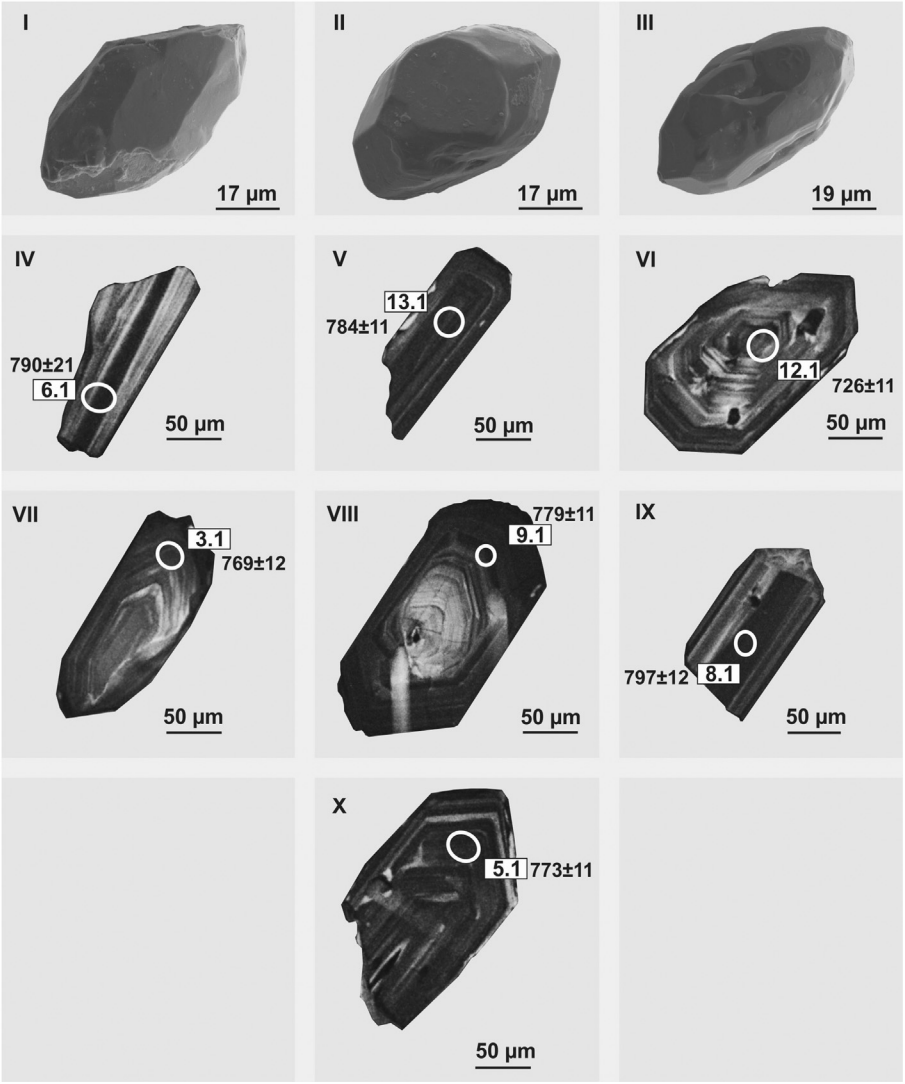

Fig. 10. Scanning electron microscopy (SEM) (I-III) and cathodoluminescence (CL) (IV-X) photographs of zircon grains from the muscovite-chlorite orthogneiss TS 1185. White circles are SHRIMP analytical spots; the numbers in the squares are in accordance with Table 3.

been dated. The isotopic data are presented in Tables 3, 4 and are plotted on the Concordia diagrams in Fig. 12.

Zircons from the Ms-Chl orthogneiss TS 1185 are transparent or translucent, euhedral, yellow and have a prismatic habit (Fig. 10). The zircons have clear magmatic zoning and in some cases contain inherited cores. The grains' sizes vary between 50 and 300 μm, and the common magmatic length/width ratio is 2.0–3.5. Eleven zircon grains were dated by SHRIMP II, and nine analyses are concordant, with a mean $^{206}Pb/^{238}U$ age of 779 ± 10 Ma (MSWD = 1.2) (Fig. 12, a). Two additional grains have younger $^{206}Pb/^{238}U$ ages and higher common Pb contents (0.47–0.62% $^{206}Pb_c$, Table 3), which may have been related to recent Pb-loss. The remaining analysis (14.2) indicates inheritance features, which could be tentatively characterized as being of Palaeoproterozoic age ($^{207}Pb/^{206}Pb$ = 1951 Ma, Table 3).

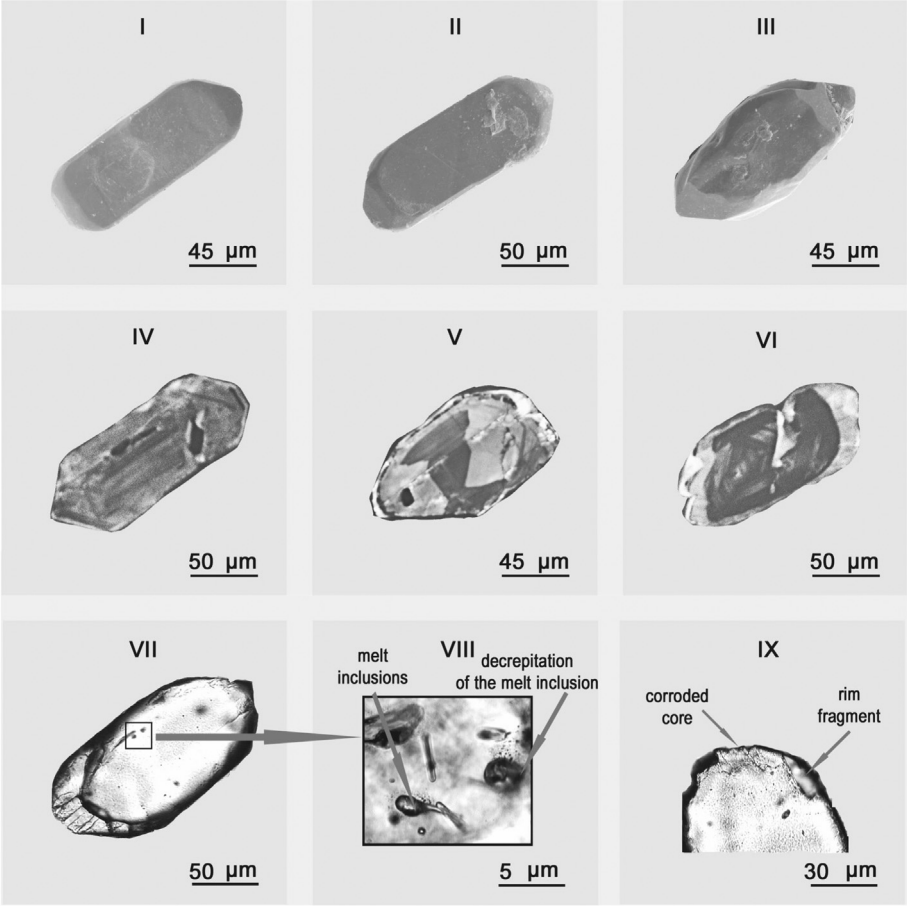

Fig. 11. SEM (I-III) and CL (IV-IX) photographs of zircon grains from the amphibole-biotite orthogneiss Z 12371.

The zircon population of the amphibole-biotite orthogneiss Z 12371 consists of subhedral, transparent or semi-transparent pale yellow or colourless prismatic grains (Fig. 11). The grain sizes range from 40 to 500 μm, with a common magmatic length/width ratio of 3.0–4.0. The zircons consist of weakly zoned cores (Figs. 11, IV-VI) and are unzoned; in some cases, they have fractured bright rims. The cores of the zircons contain abundant crystalline melt inclusions and fluid and solid inclusions of apatite, whereas the rims enclose only submicron fluid inclusions. The prisms and pyramid faces of the cores are severely corroded and are marked by fluids, bubbles and solid inclusions located in fractures (Figs. 11, VII-IX). Hence, the zircon cores display prominent magmatic features, whereas the rim origins could be apparently related to metamorphic growth. Two fractions of the cleanest untreated zircon grains as well as air-abraded and chemically abraded zircons have been analysed (analyses 1–4; Table 4), and the analytical data are well aligned on the Concordia diagram and define a discordia line (MSWD = 1.7) with intercept ages of 1841 ± 6 and 493 ± 17 Ma, respectively (Fig. 12, b). The upper intercept age of 1841 ± 6 Ma is considered to be the crystallization age of the orthogneiss protolith.

The amphibole-biotite orthogneisses have negative $\varepsilon_{Nd(t)}$ values of −4.3 to −0.1 and Neoarchean to Palaeoproterozoic Nd model ages $t_{Nd\ (DM)}$ of 2.6–2.3 Ga (Table 5; Fig. 13). The muscovite-chlorite orthogneisses are characterized by strongly negative $\varepsilon_{Nd(t)}$ values of −10.4 to −11.1 and slightly younger Palaeoproterozoic Nd model ages of 2.3–2.1 Ga. Nd whole-rock isotopic data for the AC orthogneisses suggest predominantly crustal sources of their parental melts.

3.4.2. Zircon age determinations and Sm—Nd whole-rock isotopic systematics of the garnet-mica and muscovite-chlorite schists from the KC

Cathodoluminescence images (Figs. 14, A, B) show that detrital zircons from the garnet-mica schist AH 1470 and muscovite-chlorite schist AH 1320 are typically characterized by well-preserved magmatic zoning in the cores and variable in size light-grey rims. These features suggest primary magmatic origin of zircon cores and rather metamorphic origin of the rims.

A total of 133 zircon grains from the garnet-mica schist AH 1470 were analysed and 106 concordant age estimates were obtained. Obtained zircon ages are mainly in intervals of the ranges of 667–834, 868–1051, 1087–1220, 1296–1378 and 2464–2539 Ma (Tables 5, S7) with prominent age peaks at 985 and 1151 Ma and weak peaks at 756, 822, 899, 1212, 1325, 1604, 1720, 1842 and 2507 Ma on the probability density plot (Fig. 15, A). The single grains have Ediacaran to Ordovician (632–460 Ma) and Palaeoarchean to Neoarchean (3582–2612 Ma) Concordia ages, but they do not give statistically significant age peaks (Table S7). Necessary note, that the youngest ages of 460 ± 11 and 486 ± 11 Ma were obtained for the light-grey in CL overgrowth rims, when the cores from these zircon grains yielded 975 ± 14 and 792 ± 21 Ma (Table S7).

A total of 129 zircon grains from the muscovite-chlorite schist AH 1320 were analysed and 112 concordant age estimates were obtained. The Concordia age estimates vary mainly in the intervals of 590–672, 695–790, 905–1332, 1427–1491 and 1991–2023 Ma (Tables 5, S7) with distinct age peaks at 1008 and 1081 Ma and weak peaks at 606, 638, 731, 786, 923, 1210, 1268, 1309, 1454 and 2014 Ma (Fig. 15, A).

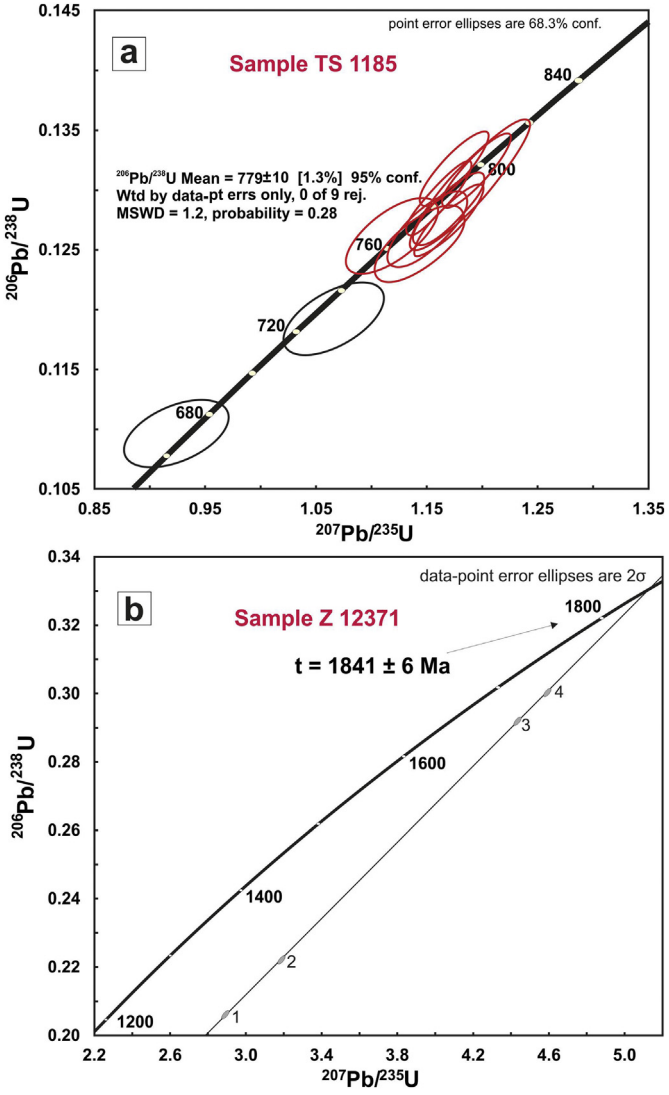

Fig. 12. U—Pb concordia diagrams, showing U—Pb isotope data of the analysed zircons: a) sample TS 1185 (SHRIMP II); b) sample Z 12371 (ID TIMS). The numbers of the points correspond to specimen numbers in Tables 3, 4.

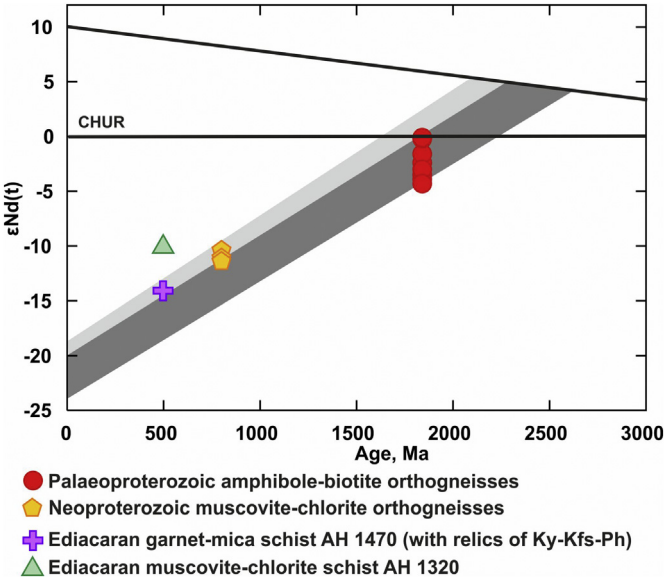

Fig. 13. Nd isotope evolution diagram for the orthogneisses of the Anrakhai Complex and the schists of the Koyandy complex, Zheltau terrane. Grey lines are evolution of isotopic compositions of the orthogneisses: light-grey line - Neoproterozoic orthogneisses; dark-grey line - Paleoproterozoic orthogneisses. CHUR is 'chondritic uniform reservoir' (Jacobsen and Wasserburg, 1984). Depleted mantle evolution curve is after Depaolo (1981).

Concordia ages of ca. 2.13, 2.32, 2.50, 2.55, 2.81, 2.96 and 3.09 Ga have been determined for the single zircon grains (Table S7).

A comparison of the obtained geochronological data in the "Overlap-Similarity" program (Gehrels et al., 2011) showed general similarity between age data from both the observed garnet-mica and muscovite-chlorite schists: degree of Similarity is 0.675 and degree of the Overlap is 0.673 (Table 6). High degree of similarity of the data is also seen on the cumulative probability curves, especially for the Neoproterozoic ages. These results imply quite similar sources of detrital zircons for the different types of metasediments of the KC.

Combined U-Th-Pb on zircon data for the garnet-mica and muscovite-chlorite schists, plotted as probability density curves (Fig. 15, A), demonstrate age peaks at 604 Ma (n = 6), 635 Ma (n = 6), 672 Ma (n = 5), 726 Ma (n = 8), 749 Ma (n = 8), 991 Ma (n = 43), 1082 Ma (n = 34), 1211 Ma (n = 7), 1272 (n = 5), 1320 Ma (n = 7), 1459 Ma (n = 4), 1604 (n = 3), 1720 (n = 3), 1843 (n = 3), 1882 (n = 3), 2014 (n = 3), 2311 (n = 3), 2506 (n = 7), 2819 (n = 3) and 2819 (n = 3). The youngest peak age of 604 Ma defines the maximum age of deposition for metasediments of the KC. Our data indicate that Archean to latest Neoproterozoic rocks were sources of the metasediments.

The garnet-mica and muscovite-chlorite schists of the KC are characterized by negative $\varepsilon_{Nd(t)}$ values ranging from −14.1 to −10.1, recalculated for the age of terrigenous protolith accumulation ca. 500 Ma and Palaeoproterozoic Nd model ages $t_{Nd(DM)}$ of 2.4–2.1 Ga (Table 5; Fig. 13).

Table 5
Sm—Nd isotopic data for the observed orthogneisses and schists from the Zheltau terrane.

Sample	Rock type	Age, Ma	Sm, ppm	Nd, ppm	$^{147}Sm/^{144}Nd$	$^{143}Nd/^{144}Nd$ (±2 σm)	$\varepsilon_{Nd}(t)$	$t_{Nd(DM)}$, Ma
TS 1185	Ms-Chl orthogneiss	800	4.60	27.07	0.1026	0.5115675	−11.3	2165
P 10091/1	Ms-Chl orthogneiss	800	3.67	19.22	0.1154	0.5116820	−10.4	2270
P 10092	Ms-Chl orthogneiss	800	4.69	30.1	0.0942	0.5115310	−11.1	2060
AH 1514	Amp-Bt orthogneiss	1840	18.01	89.5	0.1216	0.5115520	−3.5	2632
AH 1316	Amp-Bt orthogneiss	1840	18.66	94.0	0.1200	0.5115880	−2.4	2532
AH 1317/1	Amp-Bt orthogneiss	1840	14.30	84.7	0.1021	0.5114130	−1.6	2364
AH 1319	Amp-Bt orthogneiss	1840	1.21	6.63	0.1105	0.5115850	−0.2	2304
Z 12371	Amp-Bt orthogneiss	1840	18.73	92.1	0.1230	0.5115470	−3.9	2682
Z 12371/2	Amp-Bt orthogneiss	1840	7.60	40.6	0.1131	0.5116190	−0.1	2313
TS 1191/1	Amp-Bt orthogneiss	1840	16.60	83.9	0.1196	0.5115520	−3.0	2579
TS 1193/1	Amp-Bt orthogneiss	1840	12.13	61.9	0.1186	0.5114740	−4.3	2674
AH 1470	Grt-mica schist	500	6.99	35.9	0.1178	0.5116580	−14.1	2363
AH 1320	Ms-Chl schist	500	5.74	28.9	0.1204	0.5118690	−10.1	2087

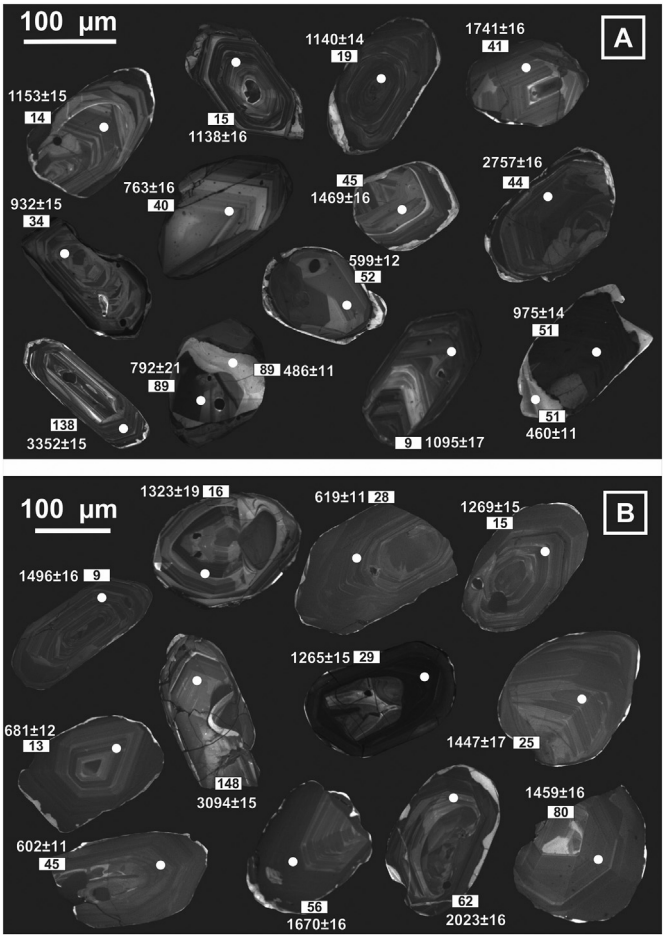

Fig. 14. CL photographs of detrital zircons from the A) garnet-mica schist AH 1470 and B) chlorite-muscovite schist AH 1320. White circles are LA-ICP MS analytical spots; the numbers in the squares and age estimates are in accordance with Table S7.

4. Discussion

The provided results (considered in Part 3 above) could shed light on the Precambrian ev
olution of the crustal complexes of the Zheltau terrane and allow correlation with the adjacent terranes from the western part of the CAOB. Previously, within the studied region, the subduction of fragments of Precambrian continental crust to high-pressure conditions in the Early Palaeozoic was proposed for the Kokchetav terrane (Okamoto et al., 2000; Katayama et al., 2001, etc.) and the Chu-Kendyktas terrane (Kröner et al., 2012; Orozbaev et al., 2010; Rojas-Agramonte et al., 2013). Alexeiev et al. (2011) suggested the possible involvement of crustal complexes of the Zheltau terrane to HP conditions, but it was not reliably proved. The conducted petrological studies allowed this suggestion to be confirmed and provided the approximate P-T paths for the principal rock types of the AC and KC.

4.1. Precambrian evolution of the Zheltau terrane

On the basis of geochronological, whole-rock geochemical and isotopic studies of the orthogneisses and schists of the AC and KC, their palaeotectonic positions and sources have been deduced. The correlation of the metamagmatic formations of the AC and metasedimentary complexes of the KC with those from the adjacent Precambrian terranes of the western CAOB has been conducted.

4.1.1. Interpretation of the zircon age estimates, whole-rock geochemical and isotopic data from the AC and KC principal rock types

A profound study of the metamorphic complexes of the Zheltau terrane showed that they were formed after igneous (anorogenic granitoids) and sedimentary rocks. As mentioned earlier, muscovite-chlorite and amphibole-biotite orthogneisses of the AC contain zircons with preserved oscillatory zoning and numerous crystalline melt inclusions, fluid and solid inclusions of apatite, indicating their magmatic derivation (Paragraph 3.4.1 above). U—Pb geochronological studies demonstrate Palaeoproterozoic (~ 1840 Ma) protolith age of the amphibole-biotite orthogneisses, whereas muscovite-chlorite orthogneisses have Neoproterozoic (~ 790 Ma) protolith age. The whole-rock Nd isotopic compositions of the Paleoproterozoic orthogneisses indicate that their protoliths were formed as a result of melting of the Neoarchean to Paleoproterozoic crustal sources probably with some juvenile material addition. Igneous protoliths of the Neoproterozoic orthogneisses were derived by partial melting of the Paleoproterozoic crustal sources as evidenced by Nd whole-rock isotopic data (Fig. 13; Table 5).

In the structure of the KC, the prevailing garnet-mica schists (strongly retrogressed Grt-Ky-Ph paragneisses) and minor muscovite-chlorite schists with bodies of marbles and metacherts, representing metasedimentary formations, possess different features in their chemical compositions and extents of metamorphic alterations. The studied detrital zircons from the schists of the KC displayed a predominant range of ages of 868–1360 Ma (135 zircon grains) with age peaks at ~ 991 Ma (n = 43) and ~ 1082 Ma (n = 34). The zircons are characterized by preserved oscillatory zoning in the cores, which is indicative of magmatic derivation. The granitoids or felsic volcanic rocks that formed at the boundary of the Late Mesoproterozoic – Early Neoproterozoic are considered as possible sources for the studied zircons. A significant role of felsic magmatic complexes in the provenance area is supported by the fractionated REE distribution spectra ($(La/Yb)_n$ = 7–15) and negative Eu anomalies (Eu/Eu^* = 0.54–0.62) (Fig. 6, C) in the schists of the KC. The whole-rock Nd isotopic compositions of the schists ($t_{Nd(DM)}$ = 2.3–2.1 Ga and $\varepsilon_{Nd(t)}$ from −14.1 to −10.1) may imply that the formation of felsic magmatic rocks of the provenance area could have resulted from melting of the Palaeoproterozoic continental crust. Noteworthy, the data collected so far indicate that Late Mesoproterozoic – Early Neoproterozoic felsic magmatic lithologies, which might have been eroded to form the protoliths of the schists of the KC, are virtually absent among the complexes of the Zheltau terrane. At the same time detrital zircons with the ages of ~ 800 Ma, corresponding to the formation age of the prevailing rocks in the AC (muscovite-chlorite orthogneisses), are sparse. This could possibly indicate that during the accumulation of the protolith of the schists of the KC, the source might have been located beyond the modern boundaries of the Zheltau terrane.

The timing of the accumulation of the protolith of the schists of the KC has been determined from the ages of detrital zircon cores. The maximum age of sedimentation corresponds to the youngest statistically significant age peak of the detrital zircon cores (~ 600 Ma), whereas the upper age limit is constrained by age of metamorphic rims in the detrital zircons from sample AH 1470 (estimated as 486 ± 11 Ma and 460 ± 11 Ma; Table S7). In summary, the accumulation of the terrigenous protolith of the observed schists was apparently in the range from ~ 600 to ~ 490 Ma, i.e., during the Ediacaran-Cambrian.

Thus, prior to Early Palaeozoic metamorphism (discussed below), Palaeoproterozoic and Neoproterozoic granitoids could be referred to the basement of the Zheltau terrane, overlain by Ediacaran-Cambrian carbonate-cherty and terrigenous cover, represented by the lithologies of the KC. It is commonly the case that Precambrian terranes of the western CAOB contain Proterozoic complexes in the basement, which are unconformably overlain by terrigenous complexes and carbonates of the Ediacaran-Cambrian cover (Degtyarev et al., 2017).

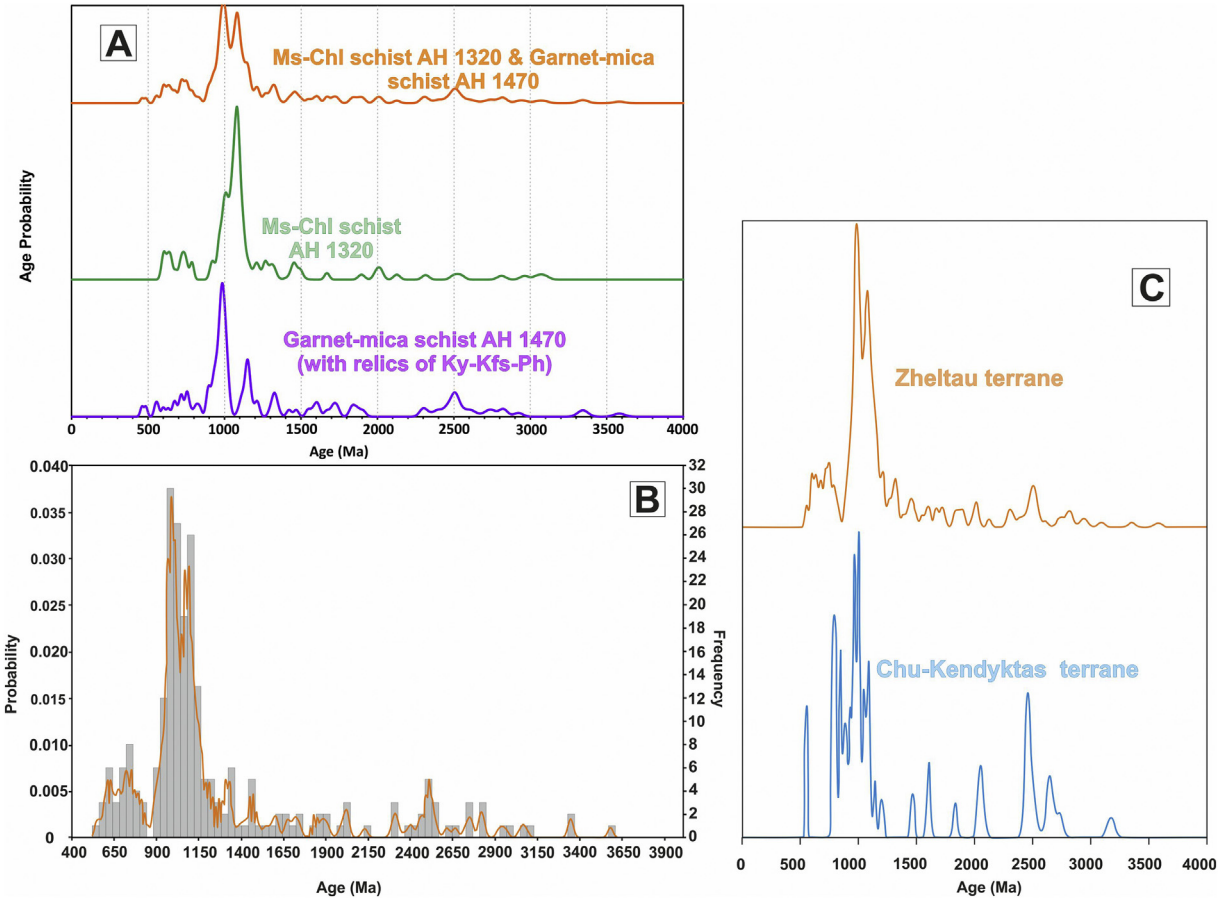

Fig. 15. A. Normalized probability plot (Gehrels et al., 2012) for detrital zircon ages from the garnet-mica and muscovite-chlorite schists of the Koyandy complex. B. Histogram and diagram of the relative probability for detrital zircon ages from the schists of the Koyandy complex in the Zheltau terrane. C. Normalized probability plot (Gehrels et al., 2012) for detrital zircon ages from the schists of the Koyandy Complex in the Zheltau terrane and the Chu-Kendyktas terrane (Tretyakov et al., 2016a).

Table 6
Results of age peaks (Gehrels et al., 2012) calculations for detrital zircons from the garnet-mica and muscovite-chlorite schists of the Koyandy Complex.

DETRITAL ZIRCON AGES AH 1470					DETRITAL ZIRCON AGES AH 1320					DETRITAL ZIRCON AGES AH 1470 + AH 1320							
MIN AGE	MAX AGE	# GRAINS	PEAK AGE	# GRAINS	MIN AGE	MAX AGE	# GRAINS	PEAK AGE	# GRAINS	MIN AGE	MAX AGE	# GRAINS	PEAK AGE	# GRAINS			
682	691	0	756	4	583	672	8	606	5	566	570	0	604	6	**OVERLAP**		
696	704	0	822	3	695	790	8	638	5	575	834	28	635	6	**AH 1470**	**AH 1470**	
729	779	3	899	5	905	1332	79	731	6	868	1360	135	672	5	**AH 1320**	0.673	**AH 1320**
791	795	1	985	23	1427	1491	3	786	3	1413	1501	6	726	8	**SIMILARITY**		
813	834	1	1151	9	1991	2023	2	923	3	1514	1528	0	749	8	**AH 1470**	**AH 1470**	
868	1051	38	1212	3				1008	19	1572	1578	0	991	43	**AH 1320**	0.675	**AH 1320**
1087	1220	13	1325	4				1081	34	1584	1614	2	1082	34			
1296	1353	4	1604	3				1210	4	1638	1644	0	1211	7			
1572	1578	0	1720	3				1268	4	1676	1705	0	1272	5			
1584	1614	2	1842	3				1309	4	1709	1736	1	1320	7			
1691	1705	0	2507	6				1454	3	1840	1904	3	1459	4			
1709	1736	1						2014	3	1991	2023	2	1604	3			
1840	1861	1								2283	2347	3	1720	3			
1869	1878	1								2419	2430	0	1843	3			
2314	2323	1								2433	2439	0	1882	3			
2419	2430	0								2464	2554	8	2014	3			
2433	2439	0								2793	2842	3	2311	3			
2464	2539	6											2506	7			
													2819	3			

4.1.2. Reconstruction of the palaeotectonic position of the Zheltau terrane in Precambrian

As indicated in Part 2, the Precambrian terranes of the western CAOB have been divided into the Issedonian (north-eastern) and Ulutau-Moyunkum (south-western) groups on the basis of the compositions and structures of Proterozoic complexes (Degtyarev et al., 2017). The Issedonian group includes the Kokchetav, Aktau-Yili, Issyk-Kul, and Chinese Central Tien Shan terranes, among others, whereas the Ulutau-Moyunkum group includes the Karatau-Talas, Chu-Kendyktas, Ulutau, Naryn-Sarydzhaz and other terranes (Fig. 1, A; Degtyarev et al., 2017). The formation and evolution of the Zheltau continental crust may have been apparently defined by an affinity to one of these groups. The results obtained by the study allowed the complexes of the Zheltau terrane to be correlated with those from other terranes of the western CAOB.

Apart from the Zheltau terrane, the Early Precambrian formations are solely known within the Naryn-Sarydzhaz (Central Tien Shan) terrane, where they comprise the Kuilu complex. It comprises Palaeoproterozoic orthogneisses with ages of 2320–2333 Ma and ~ 1850 Ma; their formation is thought to have been related to the melting of Neoarchean (2600–2700 Ma) continental crust (Kröner et al., 2017). The ages, sources and formation settings of the Palaeoproterozoic orthogneisses (1840–1850 Ma) of the Anrakhai and Kuilu complexes are very similar; hence, a mutual evolution of the Zheltau and Naryn-Sarydzhaz terranes in Early Precambrian may be suggested. Another feature indicating proximity in the Precambrian evolutions of the Zheltau and Naryn-Sarydzhaz terranes is the presence in the Anrakhai Complex of Neoproterozoic (~ 790 Ma) orthogneisses. Granitoids and felsic volcanics of similar ages are widespread within the Naryn-Sarydzhaz and other terranes of the Ulutau-Moyunkum group (Degtyarev et al., 2017; Glorie et al., 2011; Kröner et al., 2009).

The studied detrital zircons from the schists of the KC displayed another stage of magmatism at the Meso- to Neoproterozoic boundary (~ 900–1100 Ma) in the Precambrian evolution of the source, eroded during formation of the cover of the Zheltau terrane. The magmatism of the indicated period played an important role in the evolution of the Issedonian group of terranes. The formation of granitoids and felsic volcanic rocks of Precambrian terranes in Northern (~ 1200–1100 Ma) and Central (~ 920 Ma) Kazakhstan as well as Northern Tien Shan (~ 1150–1100 Ma) is thought to have been due to this stage (Degtyarev et al., 2017; Kröner et al., 2013). It has to be noted that within the Ulutau-Moyunkum group of terranes, magmatic complexes of the indicated ages have not been found. At the same time, detrital zircons with similar ages (970–1090 Ma) have been identified in the paragneisses of the Aydaly complex in the Chu-Kendyktas terrane (Tretyakov et al., 2016a) (Fig. 15, B, C).

Late Mesoproterozoic – Early Neoproterozoic magmatic complexes are present within the Tarim craton to a limited extent. The granitoids of this age are known within the NE (Quruqtagh) and eastern (Altyn-Dunhuang) parts of the craton (Lu et al., 2008; Shu et al., 2011; Zhang et al., 2013). An inferred proximity of the tectono-magmatic evolutions of the Ulutau-Moyunkum group of terranes with the Tarim craton (Degtyarev et al., 2017) allows the suggestion that the formation of the sources of detrital zircons from the schists of the Zheltau and Chu-Kendyktas terranes may have been related to magmatism in the Late Mesoproterozoic – Early Neoproterozoic, as identified within the Tarim craton or other blocks.

4.2. Early Palaeozoic metamorphism of the Zheltau terrane complexes

As considered in Paragraph 3.3, the studied lithologies of the AC and KC have undergone metamorphic alterations to various extents. From the modal compositions and mineral chemistry of the observed rock types, it is clear that the garnet-mica schists of the KC have obviously experienced at least high-pressure metamorphism and could be classified as high-pressure granulites, indicated by the presence of kyanite, phengite and K-feldspar as inclusions in garnet grains or relics in the matrix (e.g., Kotková, 2007; O'Brien and Rötzler, 2003). Previously, Alexeiev et al. (2011) indicated the presence of tiny rims in detrital zircons from the garnet-mica schists (the total population of the zircon grains is 16), which were interpreted as having grown during metamorphism but were not dated due to the sizes of the rims. In this study, 133 grains of detrital zircon in the garnet-mica schist AH 1470 were analysed; the obtained ages for metamorphic rims were tentatively estimated as 486 ± 11 Ma and 460 ± 11 Ma (Table S7). These zircon age determinations may be interpreted as the timing of high-pressure metamorphism. This is in good agreement with the zircon age estimate of 489.9 ± 3.1 Ma for garnet pyroxenites, which is considered as the time of high-pressure metamorphism (Alexeiev et al., 2011). The garnet pyroxenites with eclogites are enclosed by the garnet-mica schists (Figs. 2) and represent the strongly metamorphosed derivatives of differentiated intraplate tholeiitic melts, which were introduced into continental crust prior to subduction (Pilitsyna et al., 2018b).

Petrological studies of the garnet-mica schists have allowed the recovery of an approximate 'clockwise' P-T path for the rocks, which is common for similar complexes of subduction-collision orogens worldwide (e.g., Faryad, 2011; Li et al., 2015). Thus, sedimentary complexes were subducted to high-pressure – moderate-temperature conditions (P 15–18 kbar; T 750–850 °C) and then were exhumed with subsequent decompression. Similar scenarios have been determined for the eclogites and garnet pyroxenites distributed as pods among the garnet-mica schists (Pilitsyna et al., 2018a). Furthermore, for spinel-bearing ultramafites, which are also present as separated bodies among the migmatized garnet-mica schists (Fig. 2), the 'clockwise' P-T path has been similarly predicted; the rocks are considered as a part of the single oceanic plagioclase-bearing cumulative complex buried to the eclogite-facies field and then exhumed (Pilitsyna et al., in press). Noteworthy, that observed prograde zoning in the garnet from the high-pressure granulites, transformed to garnet-mica schists (Fig. 7, A; Part 3.3.2), which had to be obscured or modified by the processes of high-temperature diffusion, represents an example of a preserved growth zoning and indicates that these high-grade conditions *did not last long*. There is a large number of high-pressure terranes worldwide, formation of which is thought to have been attributed to the subduction-collisional settings (e.g. Iberian massif, Spain (Escuder-Viruete et al., 2000), Moldanubian Zone, Czech Republic (O'Brien and Vraná, 1995), Moldanubian Zone, Austria (Cooke et al., 2000), etc.), where high-pressure rocks contain a number of minerals, preserving the features of the prograde-to-peak P-T evolution, including garnet with a prominent bell-shaped Mn profile, which is also observed in the garnet-mica schists of the KC in the Zheltau terrane. Hence, it has been deduced that the studied garnet-mica schists and the enclosed eclogites/garnet pyroxenites as well as spinel-bearing ultramafites could share a single 'clockwise' P-T-t history, reflecting the involvement of different horizons of continental and oceanic crust into the subduction process and their subsequent mutual exhumation in the subduction channel, as indicated by the characteristic block-in-matrix structure of the metamorphic complexes.

In such a case, the muscovite-chlorite schists (which do not contain index-minerals of high-pressure origin or even garnet but share the single complex with the above observed garnet-mica schists) were evidently formed after sedimentary rocks, which were buried up to relatively shallow depths and avoided high-pressure metamorphism. It is also confirmed by field observations, where the muscovite-chlorite schists are found in association with the low-grade amphibolites (without garnet) and metacherts with marbles (Fig. 2). However, the rocks could be exhumed together with the garnet-mica schists and ultramafites, eventually forming tectonic slice packages. In addition, in all the analysed grains of detrital zircon from the muscovite-chlorite schist AH 1320, metamorphic rims are either utterly thin or more commonly absent; this could also indicate the low grade of metamorphic alteration of the rocks.

Metamorphic alterations of the Neoproterozoic muscovite-chlorite and Palaeoproterozoic amphibole-biotite orthogneisses are not very representative for recovering the P-T history of the rocks. Nonetheless, assuming that protoliths of the orthogneisses along with the above considered metasedimentary complexes represented parts of the single terrane in the Precambrian (as indicated earlier in Paragraph 4.1), it is strongly possible that the observed orthogneisses were also subducted in the Early Palaeozoic. However, it is unlikely that solely the cover of the terrane (garnet-mica schists) experienced high-pressure metamorphism, whereas the basement avoided a burial to high-pressure conditions. From here, we suppose, that at least minor part of the orthogneisses of the AC together with the mica-schists of the KC indeed experienced high-pressure metamorphism with the following migmatization (diatexite formation), but the robust evidences are virtually absent in the rocks up to date and additional geological and petrological studies are of great interest. Instead, in accordance with pseudosection modelling (Supplementary Fig. S5), an assemblage of Mn-rich garnet with hastingsite in the Palaeoproterozoic Amp-Bt orthogneisses was formed under epidote-amphibolite facies conditions. Metamorphic changes of the rocks are also supported by the presence of thin rims around the zircon cores (Fig. 11). The subsequent development of chlorite and actinolite in the cracks of the hastingsite crystals may indicate decompression in the low-grade green-schist facies field, implying a 'clockwise' P-T evolution for these rocks. In the Neoproterozoic muscovite-chlorite orthogneisses, relics of biotite among abundant chlorite are occasionally preserved, which may also be interpreted as a retrogression from epidote-amphibolite facies to the lower stages of metamorphism.

In summary, it can be deduced that the studied Precambrian formations of the AC (orthogneisses) and KC (schists) comprising the Zheltau terrane mutually underwent pervasive metamorphic alterations during subduction in the Early Palaeozoic. However, only a minor part of the exposed lithologies indeed experienced high-pressure conditions (garnet-mica schists with pods of eclogites, garnet pyroxenites and spinel ultramafites, possibly migmatized orthogneisses (?)), whereas the greater part of the observed formations was buried to considerably shallower levels. Nevertheless, the spatial proximity of the studied complexes in the field and similar metamorphic changes in the latest stages of retrogression imply their possible mutual exhumation from different levels and subsequent juxtaposition as a package of tectonic slices. The exhumation evidently occurred in the period between 490 Ma (metamorphic peak) and 470 Ma, since the metamorphic complexes of the Zheltau terrane are overlain by Early and Middle Ordovician terrigenous and silicic strata (Nedovizin, 1961; Tolmacheva, 2014). Exhumation rates are estimated by an uplift time to the near-face of middle crustal levels of ~ 15 km as ~ 3.5–4 mm/year (after Ernst et al., 1997), which may have been generally considered as fairly fast rates of exhumation, consistent to those from other UHP-HP terranes worldwide.

4.3. Geodynamic evolution of the Zheltau terrane in the latest Cambrian-Early Ordovician

The main geological events, related to the Early Palaeozoic metamorphism of the Precambrian complexes of the Zheltau terrane (discussed in Part 4.2) and their subsequent exhumation to the upper horizons, took place in the latest Cambrian-Early Ordovician. In the late Cambrian the Zheltau terrane represented a Precambrian block, the basement of which was composed of the Paleoproterozoic (~ 1840 Ma) and Neoproterozoic (~ 800 Ma) orthogneisses with amphibolites, whereas the Ediacaran-Cambrian cover of the terrane was made up by mainly terrigenous formations with layers and lenses of carbonates and cherts. A number of bodies of layered gabbroids were evidently attributed to the complexes of the cover (Pilitsyna et al., 2018b). In the early-middle Cambrian the Zheltau terrane (or microcontinent) was separated from the Chu-Kendyktas and Aktau-Yili terranes by new-formed oceanic basins from the SW and NE (in modern coordinates). Pre-late Cambrian evolution and possible settings of these oceanic basins formation are described in details in Pilitsyna et al. (in press).

In the latest Cambrian-early Tremadocian (~ 490–485 Ma) a closure of the oceanic basins, separating the indicated microcontinents, was initiated. In the Dzhalair-Naiman basin, separating the Chu-Kendyktas and Zheltau microcontinents (Supplementary Fig. S7, a), tectonic converging of the older oceanic complexes, overlain by early Tremadocian flysch, took place. Obduction of the oceanic complexes onto the Chu-Kendyktas microcontinent, accompanied by formation of the several large allochthones (e.g. Kopurelisay complex in the Aktyuz block (Kröner et al., 2012)) and their subsequent erosion with accumulation of the ophiolitic clastic material (Ryazantsev et al., 2009) also occurred. During this period a closure of the oceanic basin, separating the Zheltau and Aktau-Yili microcontinents, was completed. At the same time a tectonic dismembering of the Zheltau microcontinent crust into several tectonic slices with burying to the different depths under the Aktau-Yili microcontinent, took place. Tectonic slice, composed of the rocks of the Koyandy Complex together with formations of the Anrakhai Complex and upper mantle-lower crustal oceanic formations, was buried to the mantle depths of ~ 70 km, were garnet clinopyroxenites, eclogites, spinel-bearing peridotites, garnet-kyanite-bearing high-pressure granulites were formed. At the same time, the most part of the complexes of the Zheltau microcontinent was buried to shallower depths, which did not exceed the amphibolite facies conditions.

In the Early Ordovician (~ 480–475 Ma) (Supplementary Fig. S7, b) the Dzhalair-Naiman oceanic basin was completely closed; on its place the strongly deformed suture zone, composed of Cambrian ophiolites with island-arc complexes and Early Ordovician flysh, was formed. Some fragments of the Chu-Kendyktas microcontinent (the Aktyuz complex of the cognominal block (Fig. 1, A)) were buried under the Zheltau microcontinent up to the depths of ~ 70–80 km, where eclogites with high-pressure gneisses were formed and then subsequently exhumed (Kröner et al., 2012). In the suture zone, separating the Zheltau and Aktau-Yili microcontinents, a buoyancy-driven relatively fast exhumation of the metamorphic complexes from the different horizons after slab break-off took place.

5. Conclusions

1. Metamagmatic felsic rocks of the Zheltau terrane (the Anrakhai Complex) are represented by predominant Neoproterozoic muscovite-chlorite orthogneisses with the protolith age of ca. 790 Ma and subordinate Palaeoproterozoic amphibole-biotite orthogneisses with the age of protolith formation ~ 1840 Ma;
2. Anorogenic granitoids are thought to represent the protoliths of the Palaeoproterozoic and Neoproterozoic orthogneisses. The protolith of the Palaeoproterozoic amphibole-biotite orthogneisses was formed as a result of a mixing of a Neoarchean crustal source with a juvenile source, whereas the formation of the Neoproterozoic muscovite-chlorite orthogneisses' protolith may have been related to the melting of Palaeoproterozoic crustal material;
3. The studied metasedimentary rocks of the Zheltau terrane (the Koyandy Complex) are represented by prevailing garnet-mica schists and minor muscovite-chlorite schists. Detrital zircons from the schists displayed a predominant range of ages of 604–2819 Ma with two maximum peaks at ~ 991 Ma and ~ 1082 Ma. Nd whole-rock isotopic and U-Th-Pb on zircon geochronological data imply derivation of protoliths of the garnet-mica and muscovite-chlorite schists from mainly Paleoproterozoic and Archean sources reworked in Meso- and Neoproterozoic;
4. Granitoids or felsic volcanic rocks that formed at the boundary of the Late Mesoproterozoic – Early Neoproterozoic are considered to be possible sources for the studied detrital zircons from the schists. The formation of these felsic rocks is thought to have resulted from the melting of Palaeoproterozoic continental crust. The accumulation of the terrigenous protolith of the garnet-mica and muscovite-

chlorite schists of the Koyandy Complex apparently occurred in the range from ~ 600 to ~ 490 Ma, corresponding to the Ediacaran-Cambrian.

5. Protoliths of the Palaeoproterozoic and Neoproterozoic orthogneisses of the Anrakhai Complex comprised the basement of the Zheltau terrane in Precambrian, whereas the protoliths of the schists of the Koyandy Complex evidently represented the terrigenous cover. Different horizons of Precambrian crust of the Zheltau terrane were subducted to moderate- and high-grade conditions in the Early Palaeozoic. The garnet-mica schists have evidently experienced high-pressure – moderate-temperature metamorphism (P 15–18 kbar; T 750–850 °C) and represent strongly retrogressed high-pressure granulites, whereas the muscovite-chlorite schists and the orthogneisses of the Anrakhai Complex (at least the most part of them) avoided high-pressure re-equilibration.

Supplementary data to this article can be found online at https://doi.org/10.1016/j.lithos.2018.10.033.

Qz – quartz; Pl – plagioclase; Kfs – K-feldspar; Chl – chlorite; Grt – garnet; Bt – biotite; Ms. – muscovite; Ph – phengite; Ky – kyanite; Tur – tourmaline.

Chondrite and primitive mantle values are from Sun and McDonough (1989). PAAS composition is from Taylor and McLennan (1985).

Acknowledgements

A.P. is thankful to James Connolly for his kind help with the pseudosection modelling. We are grateful to I.A. Anisimova, A.M. Fedoseenko and Emily C.H. Hung, who helped with the analytical works in the laboratories. We are grateful to both anonymous reviewers for their valuable and reasonable comments and sincere attention to the manuscript. We also thank Dr. Hafiz U. Rehman for invitation to the SI and his kind support. The analytical procedures for the study and expedition works were funded by research project № 14-27-00058 of the Russian Science Foundation. The study was also funded by the research projects of Russian Foundation of the Basic Research RFBR № 17-05-00357 and № 18-35-00199. Parts of U—Pb geochronological studies have been supported by Ministry of Science and Technology of Taiwan (MOST 104-2923-M-001-003-MY3).

Appendix A. Appendix A. Analytical methods for whole-rock and mineral chemistry determinations

A.1. Whole-rock geochemistry

Major elements were determined by XRF using a Bruker AXS wavelength dispersive S4 PIONEER spectrometer with a 4 kW X-ray tube at the Geological Institute of the Russian Academy of Sciences (RAS). Data processing was implemented using the «Spectra-Plus^{TM}» software package. The automatic registration of peak overlaps and correction for matrix effects were carried out during individual measurements of fundamental parameters for each sample. The intervals of analysed concentrations obtained after recalculation to oxides (mass fraction %) were Si – 0.01–1.0, Ti – 0.01–5.0, Al – 1.0–60.0, Fe (total) – 1.0–40.0, Mn – 0.01–1.0, Ca – 1.0–50, Mg – 0.1–40, Na – 0.1–10.0, K – 0.1–10.0, and P – 0.01–5.0. Ferric and ferrous iron were calculated using the HCAM 50-X titrimetric bichromatic method (Kazakhstan Institute of Metrology; reg. number KZ.07.00.03141-2015 from 12.05.2015).

Trace elements were acquired by the Analytical Centre of the Institute of Microelectronics Technology and High-Purity Materials RAS using an ICP-MS on a Perkin Elmer ELAN 6100 DRC as well as by atomic emission spectrometry with ICP-MS (ICAP-61, Thermo Jarrell Ash; X-7, Thermo Elemental, USA). The relative standard deviation for all analysed elements was no more than 0.2 for element contents below the five-fold detection limit and below 0.1 for contents above the five-fold detection limit.

The major element concentrations are given in wt.%, and the trace elements are given in ppm in Table 2.

A.2. Mineral chemistry

Mineral compositions were determined using a JEOL-8200 electron probe microanalyser (EPMA) in the Laboratory of Mineral Substances Analysis, Institute of Mineralogy, Geochemistry and Petrography of the RAS and a JEOL JXA-8230 EPMA at the Institut des Sciences de la Terre (ISTerre, University Grenoble Alpes, France). These were equipped with five wavelength dispersive spectrometers and an energy dispersive (EDX) spectrometer operating at an accelerating voltage of 20 kV, probe current of 20 nA, and beam diameter of 1 μm. The standards were certified natural minerals and synthetic oxides: Wollastonite (Si, Ca), Corundum (Al), Orthoclase (K), Rhodonite (Mn), Albite (Na), Apatite (P), Rutile (Ti), Hematite (Fe), and Periclase (Mg). Ferric iron was recalculated for garnet and amphibole on the basis of charge balance and stoichiometry (Droop, 1987). Mineral abbreviations are after Whitney and Evans (2010); a.p.f.u. is 'atom per formula unit'.

Appendix B. Appendix B. Pseudosection modelling

Perple_X software (version 6.7.3; Connolly (1990), Connolly (2005)) in conjunction with the internally consistent thermodynamic database of Holland and Powell (1998) for CaO-FeO-MgO-MnO-Na_2O-K_2O-Al_2O_3-SiO_2-H_2O (amphibole-biotite orthogneiss Z 12371(Fig. S5; Table 2)) and CaO-FeO-MgO-MnO-Na_2O-K_2O-Al_2O_3-TiO_2-SiO_2-H_2O (garnet-mica schists AH 1470 and Z 12375 (Fig. 9, S6; Table 2)) systems were used to construct pseudosections. Total iron was taken to avoid additional uncertainties in calculations; in accordance with stoichiometry the contents of Fe^{3+} in the principal phases (e.g. garnet, biotite, amphibole) are supposed to be negligible.

Since the garnet of the schist AH 1470 reveals preserved prograde zonation with decreasing Mn from core to rims (Fig. 7, A), the measured whole-rock composition of the sample was introduced to roughly estimate the pressure-temperature parameters of the prograde stage for the rock (Table 2). However, it must be cautioned that the sample demonstrates pervasive retrograde alterations, related to development of biotite-muscovite-Ca-rich plagioclase aggregates around garnet grains. This could contribute the significant changes to initial reacting bulk composition, responsible for the prograde garnet growth. Besides manganese-rich cores of garnets of the prograde stages are commonly enriched in ferric iron, which was not taken into consideration in this study. Garnets from the schist Z 12375 are characterized by diffusion zoning, implying P-T parameters of their formation within the high grade of metamorphism; from here it was suggested that the garnets could have formed in equilibrium with high-pressure and high-temperature phases, and the measured whole-rock composition of the sample corresponds to some extent to the reacting bulk during the near-peak and post-peak evolution of the rock. Therefore, the measured whole-rock composition of the sample Z 12375 was used to assess the approximate P-T paths for the near-peak (mantle parts of garnet grains) and post-peak retrograde (mantle-rim parts of garnet grains) stages (Table 2).

The following solution models were incorporated: Gt(HP) for garnet (Holland and Powell, 1998), Bio(HP) for biotite (Powell and Holland, 1999), Mica(CHA) for white mica (Coggon and Holland, 2002; Auzanneau et al., 2010), feldspar for plagioclase and potassium feldspar (Fuhrman and Lindsley, 1988), and melt (HP) for haplogranitic melt (Holland and Powell, 2001; White et al., 2001). H_2O is considered as the saturated phase for the prograde stage (CORK equation of state (Holland and Powell, 1998)); at the peak stage, melt commencement is referred (with subsequent propagation of the melt volume during the retrogression), and therefore H_2O is taken as a system component

equal to the loss on ignition value for the peak and retrograde stages (Table 2).

For the amphibole-biotite orthogneiss Z 12371, the measured whole-rock bulk composition was used (Table 2). The following solution models were incorporated: Gt(HP) for garnet (Holland and Powell, 1998), Amph(DHP) for amphibole (Dale et al., 2000), Bio(HP) for biotite (Powell and Holland, 1999), Mica(CHA) for white mica (Coggon and Holland, 2002; Auzanneau et al., 2010), feldspar for plagioclase and potassium feldspar (Fuhrman and Lindsley, 1988). H_2O was added as a saturated phase and recalculated using the CORK equation of state (Holland and Powell, 1998).

The compositional isopleths for all pseudosections were plotted using PyWerami software (Lexa, 2011).

Appendix C. Appendix C. Analytical technique for zircon age determinations and Sm-Nd whole-rock isotopic analysis

The U-Pb ID-TIMS isotope investigations were carried out in the laboratory of Isotope Geology, Institute of Precambrian Geology and Geochronology RAS. Zircon morphology and internal structure were studied with an ABT 55 scanning electron microscopy with CL detector and LEICA DMLP microscope. The zircon grains selected for study were washed in alcohol, acetone, and 1 M HNO_3. Chemical abrasion was performed with a mixture of HF and HNO_3 (10:1) at 220 °C for 2 and 4 hours, respectively (Mattinson, 1994). The dissolved parts of the zircons were decanted, and the residues were rinsed with concentrated HCl overnight and then several times on a hot plate with fresh portions of acid. The residues were then spiked, dissolved and analysed following the method of Krogh (1973). Before decomposition, the zircons were spiked with a mixed ^{202}Pb - ^{235}U spike. Digestion of the zircons and U and Pb extractions were performed following a modified technique of Krogh (1973). The isotope analyses were performed using a TRITON TI multicollector mass spectrometer in static and dynamic (with an electron multiplier) modes. The analytical uncertainties of the U and Pb concentrations were 0.5%, and the blanks were less than 10 pg for Pb and 1 pg for U. The raw data were processed using PbDAT (Ludwig, 1989) and ISOPLOT (Ludwig, 2012). Common Pb correction was applied according to the model of Stacey and Kramers (1975). All errors are reported as 2σ means.

The SIMS U-Pb isotope analyses of zircon separates were carried out using a SHRIMP-II ion probe at the Center for Isotope Research of the Karpinsky Russian Geological Research Institute following conventional techniques (Williams, 1998; Larionov et al., 2004). The zircons were mounted in epoxy along with the zircon standards 91500 (Wiedenbeck et al., 1995) and Temora (Black et al., 2003), polished to approximately half of the grain thicknesses and coated with 99.999% pure gold. The inner structure of the zircons was examined using optical microscopy and cathodoluminescence. Regions devoid of visible cracks and inclusions in euhedral crystals were chosen for analysis. The data were processed with the SQUID v1.12 and ISOPLOT/Ex 3.22 (Ludwig, 2005a; 2005b) programs using the decay constants of Steiger and Jäger (1977). The correction for common Pb was applied according to the model of Stacey and Kramers (1975) using the measured $^{204}Pb/^{206}Pb$ ratio.

Zircon U-Th-Pb isotopic data for samples AH 1470 and AH 1320 were obtained using the *LA-ICP-MS technique* at the Department of Geosciences, National Taiwan University (NTU), Taipei, using an Agilent 7500s quadrupole ICP-MS and a NewWave UP213 laser ablation system. The detailed analytical procedures can be found in Chiu et al. (2009). During the experiments, about 1 min was spent for measuring the gas blank, and the results indicate a sensitivity of less than 1000 counts per second for all measured isotopes. Spot analyses were done using a spot diameter of 30 μm. Calibration was performed using the GJ-1 zircon standard, with a well-established $^{207}Pb/^{206}Pb$ age and an intercept age, using isotope dilution thermal ionization mass spectrometry (ID-TIMS), of 608.5 ± 0.4 Ma (2σ) and 608.5 ± 1.5 Ma (2σ), respectively (Jackson et al., 2004). The Harvard 91500 Wiedenbeck et al. (1995) and Plešovice (PLS) (Sláma et al., 2008) reference zircons were used as secondary standards for data quality control. All U-Th-Pb isotopic ratios were calculated using the GLITTER 4.0 (GEMOC) software (Van Achterbergh et al., 2001), and common lead was corrected using the common lead correction function proposed by Anderson (2002). Concordia ages were calculated using Isoplot v. 4.15 (Ludwig, 2008). Only Concordia ages with MSWD < 1 were used for construction of histograms, probability density plots and calculation of age peaks (Gehrels, 2012).

Our $^{207}Pb/^{235}U$, $^{206}Pb/^{238}U$ and $^{207}Pb/^{206}Pb$ ages of zircon 91500 obtained in the NTU are 1059 ± 8 Ma, 1055 ± 9 Ma and 1068 ± 10 Ma (2σ), respectively, which are in good agreement with the values reported by Wiedenbeck et al. (1995) using ID-TIMS methods. Our weighted average of $^{206}Pb/^{238}U$ ages for the PLS zircon is 336 ± 3 Ma (2σ, MSWD = 0.25, Probability = 1.00) and match the corresponding age of 337.13 ± 0.37 Ma recommended by (Sláma et al., 2008).

Whole-rock Sm-Nd isotopic analyses were performed at the Institute of Precambrian Geology and Geochronology, RAS, St. Petersburg. Approximately 100 mg of whole-rock powder were dissolved in a mixture of HF, HNO_3 and $HClO_4$. A ^{149}Sm–^{150}Nd spike solution was added to samples prior to dissolution. The REE were separated on BioRad AGW50-X8 200-400 mesh resin using conventional cation-exchange techniques. Sm and Nd were separated by extraction chromatography using a LN-Spec (100–150 mesh) resin. The total laboratory blanks were 0.1–0.2 ng for Sm and 0.1–0.5 ng for Nd. Isotopic compositions of Sm and Nd were measured on a TRITON TI multi-collector mass-spectrometer in static mode. The precision (2σ) of Sm and Nd contents and $^{147}Sm/^{144}Nd$ ratios was ca. 0.5% and ca. 0.005% for the $^{143}Nd/^{144}Nd$ ratios. $^{143}Nd/^{144}Nd$ ratios were normalized against $^{146}Nd/^{144}Nd$ = 0.7219 and adjusted relative to a value of 0.512115 for the JNdi-1 standard (Tanaka et al., 2000). During the period of analysis, the weighted average of 7 JNdi-1 Nd standard runs yielded 0.512101 ± 5 (2σ).

The $\varepsilon_{Nd(t)}$ values were calculated using the present-day values for a chondritic uniform reservoir (CHUR) $^{143}Nd/^{144}Nd$ = 0.512638 and $^{147}Sm/^{144}Nd$ = 0.1967 (Jacobsen and Wasserburg, 1984). Whole-rock Nd $t_{(DM)}$ model ages were calculated using the model of Goldstein and Jacobsen (1988), according to which the Nd isotopic composition of the depleted mantle evolved linearly since 4.56 Ga ago and has a present-day value $\varepsilon_{Nd(0)}$ of +10 ($^{143}Nd/^{144}Nd$ = 0.513151 and $^{147}Sm/^{144}Nd$ = 0.21365).

References

Alexeiev, D.V., Ryazantsev, A.V., Kröner, A., Tretyakov, A.A., Xia, X., Liu, D.Y., 2011. Geochemical data and zircon ages for rocks in a high-pressure belt of Chu-Yili Mountains, southern Kazakhstan: Implications for the earliest stages of accretion in Kazakhstan and the Tianshan. J. Asian Earth Sci. 42, 805–820. https://doi.org/10.1016/j.jseaes.2010.09.004.

Anderson, T., 2002. Correction of common lead in U-Pb analyses that do not report ^{204}Pb. Chem. Geol. 192, 59–79. https://doi.org/10.1016/S0009-2541(02)00195-X.

Auzanneau, E., Schmidt, M.W., Vielzeuf, D., Connolly, J.A.D., 2010. Titanium in phengite: a geobarometer for high temperature eclogites. Contrib. Mineral. Petrol. 159, 1–24. https://doi.org/10.1007/s00410-009-0412-7.

Barker, F., 1979. Trondhjemite: definition, environment and hypotheses of origin. In: Barker, F. (Ed.), Trondhjemites, Dacites, and Related Rocks. Elsevier, New York, pp. 1–12.

Black, L.P., Kamo, S.L., Allen, C.M., Aleinikoff, J.N., Davis, D.W., Korsch, R.J., Foudoulis, C., 2003. TEMORA 1: a new zircon standard for Phanerozoic U-Pb geochronology. Chem. Geol. 200, 155–170. https://doi.org/10.1016/S0009-2541(03)00165-7.

Carswell, D.A., Harvey, M.A., Al-Samman, A., 1983. The Petrogenesis of constraining Fe-Ti and Mg-Cr garnet peridotite types in the high grade gneiss complex of Western Norway. Bull. Mineral Res. Explor. 106, 727–750.

Chiu, H.-Y., Chung, S.-L., Wu, F.-Y., Liu, D., Liang, Y.-H., Lin, I.-J., Iizuka, Y., Xie, L.-W., Wang, Y., Mei-Fei Chu, M.-F., 2009. Zircon U-Pb and Hf isotopic constraints from eastern Transhimalayan batholiths on the precollisional magmatic and tectonic evolution in southern Tibet. Tectonophysics 477 (1–2), 3–19. https://doi.org/10.1016/j.tecto.2009.02.034.

Coggon, R., Holland, T.J.B., 2002. Mixing properties of phengitic micas and revised garnet-phengite thermobarometers. J. Metamorph. Geol. 20, 683–696. https://doi.org/10.1046/j.1525-1314.2002.00395.x.

Connolly, J.A.D., 1990. Multivariable phase-diagrams: an algorithm based on generalized thermodynamics. Am. J. Sci. 290, 666–718. https://doi.org/10.2475/ajs.290.6.666.

Connolly, J.A.D., 2005. Computation of phase equilibria by linear programming: a tool for geodynamic modeling and its application to subduction zone decarbonation. Earth Planet. Sci. Lett. 236 (1), 524–541. https://doi.org/10.1016/j.epsl.2005.04.033.
Cooke, R.A., O'Brien, P.G., Carswell, D.A., 2000. Garnet zoning and the identification of equilibrium mineral compositions in high-pressure–temperature granulites from the Moldanubian Zone, Austria. J. Metamorph. Geol. 18, 551–569. https://doi.org/10.1046/j.1525-1314.2000.00273.x.
Dale, J., Holland, T., Powell, R., 2000. Hornblende-garnet-plagioclase thermobarometry: a natural assemblage calibration of the thermodynamics of hornblende. Contrib. Mineral. Petrol. 140, 353–362. https://doi.org/10.1007/s004100000187.
Degtyarev, K.E., 2012. Tectonic Evolution of Early Paleozoic Island-arc Systems and Formation of Caledonides Continental Crust in Kazakhstan. GEOS, Moscow (289 pp., in Russian).
Degtyarev, K.E., 2012. Tectonic Evolution of Early Paleozoic Island-Arc Systems and Formation of Caledonides Continental Crust in Kazakhstan. Vol. 289. GEOS, Moscow (p. in Russian).
Degtyarev, K.E., Ryazantsev, A.V., Tretyakov, A.A., Tolmacheva, T.Yu., Yakubchuk, A.S., Kotov, A.B., Salnikova, E.B., Kovach, V.P., 2014. Neoproterozoic to early Paleozoic tectonic evolution of the western part of the Kyrgyz Ridge Caledonides (North Tianshan). Geotectonics 47 (6), 377–417. https://doi.org/10.1134/S0016852113070017.
Degtyarev, K., Yakubchuk, A., Tretyakov, A., Kotov, A., Kovach, V., 2017. Precambrian geology of the Kazakh Uplands and Tien Shan: an overview. Gondwana Res. 47, 44–75. https://doi.org/10.1016/j.gr.2016.12.014.
Depaolo, D.J., 1981. Neodymium isotopes in the Colorado Front Range and crust-mantle evolution in the Proterozoic. Nature 291, 193–196. https://doi.org/10.1038/291193a0.
Droop, T.R.G., 1987. A general equation for estimating Fe^{3+} concentrations in ferromagnesian silicates and oxides from microprobe analyses, using stoichiometric criteria. Mineral. Mag. 51, 431–435. https://doi.org/10.1180/minmag.1987.051.361.10.
Eby, N.G., 1992. Chemical subdivision of the A-type granitoids: petrogenetic and tectonic implications. Geology 20, 641–644 (10.1130/0091-7613(1992)020<0641:CSOTAT>2.3.CO;2).
Efimov, I.A., Borovinskaya, L.G., Naydenov, B.M., 1983. Eclogites of Southern Kazakhstan and their Radiologic Age. Problems of Metallogeny of Kazakhstan. Alma-Ata, pp. 81–115 (in Russian).
Ernst, W. G., Maruyama, S., Wallis, S., 1997. Buoyancy-driven, rapid exhumation of ultrahigh-pressure. metamorphosed continental crust. Geology 94 (18), 9532–9537.
Escuder-Viruete, J., Indares, A., Arenas, R., 2000. P–T paths derived from garnet growth zoning in an extensional setting: an example from the Tormes Gneiss Dome (Iberian Massif, Spain). J. Petrol. 41 (10), 1489–1515.
Faryad, S.W., 2011. Distribution and geological position of high-/ultrahigh-pressure units within the European Variscan Belt: a review. In: Dobrzhinetskaya, L., Faryad, S.W., Wallis, S., Cuthbert, S. (Eds.), Ultrahigh Pressure Metamorphism: 25 Years After the Discovery of Coesite and Diamond. Elsevier, pp. 361–397 https://doi.org/10.1016/B978-0-12-385144-4.00011-4.
Frost, C.D., Frost, B., 2011. On ferroan (A-type) granites: their compositional variability and modes of origin. J. Petrol. 52, 39–53. https://doi.org/10.1093/petrology/egq070.
Frost, B.R., Barnes, C.G., Collins, W.J., Arculus, R.J., Ellis, D.J., Frost, C.D., 2001. A geochemical classification for granitic rocks. J. Petrol. 42, 2033–2048. https://doi.org/10.1093/petrology/42.11.2033.
Fuhrman, M.L., Lindsley, D.H., 1988. Ternary-feldspar modeling and thermometry. Am. Mineral. 73, 201–215.
Ganguly, J., Saxena, S.K., 1984. Mixing properties of aluminosilicate garnets: constraints from natural and experimental data, and applications to geothermobarometry. Am. Mineral. 69 (1–2), 88–97.
Gehrels, G.E., 2012. Detrital zircon U-Pb geochronology: current methods and new opportunities. In: Busby, C., Azor, A. (Eds.), Tectonics of Sedimentary Basins: Recent Advances. Wiley-Blackwell, Chichester, UK, pp. 47–62. https://doi.org/10.1002/9781444347166.ch2.
Glorie, S., De Grave, J., Buslov, M.M., Zhimulev, F.I., Stockli, D.F., Batalev, V.Y., Izmer, A., Van den Haute, P., Vanhaecke, F., Elburg, M.A., 2011. Tectonic history of the Kyrgyz South Tianshan (Atbashi-Inylchek) suture zone: the role of inherited structures during deformation-propagation. Tectonics 30 (6), TC6016. https://doi.org/10.1029/2011TC002949.
Goldstein, S.J., Jacobsen, S.B., 1988. Nd and Sr isotopic systematics of rivers water suspended material: implications for crustal evolution. Earth Planet. Sci. Lett. 87, 249–265. https://doi.org/10.1016/0012-821X(88)90013-1.
Hammarstrom, J.M., Zen, E., 1986. Aluminum in hornblende: an empirical igneous geobarometer. Am. Mineral. 71, 1297–1313.
Henry, D.J., Novák, M., Hawthorne, F.C., Ertl, A., Dutrow, B.L., Uher, O., Pezzotta, F., 2011. Nomenclature of the tourmaline-supergroup minerals. Am. Mineral. 96, 895–913. https://doi.org/10.2138/am.2011.3636.
Herron, M.M., 1988. Geochemical classification of terrigenous sands and shales from core or log data. J. Sediment. Res. 58 (5), 820–829. https://doi.org/10.1306/212F8E77-2B24-11D7-8648000102C1865D.
Holland, T.J.B., Powell, R., 1998. An internally consistent thermodynamic data set for phases of petrological interest. J. Metamorph. Geol. 16, 309–343. https://doi.org/10.1111/j.1525-1314.1998.00140.x.
Holland, T., Powell, R., 2001. Calculation of phase relations involving haplogranitic melts using an internally consistent thermodynamic dataset. J. Petrol. 42, 673–683. https://doi.org/10.1093/petrology/42.4.673.
Hollister, L.S., Grissom, G.C., Peters, E.K., Stowell, H.H., Sisson, V.B., 1987. Confirmation of the empirical correlation of Al in hornblende with pressure of solidification of calc-alkaline plutons. Am. Mineral. 72, 231–239.
Indares, A., 1995. Metamorphic interpretation of high-pressure-temperature metapelites with preserved growth zoning in garnet, eastern Grenville Province, Canadian Shield. J. Metamorph. Geol. 13, 475–486. https://doi.org/10.1111/j.1525-1314.1995.tb00235.x.
Indares, A., Dunning, G., 2001. Partial melting of high-P-T metapelites from the Tshenukutish Terrane (Grenville Province): petrography and U-Pb dating. J. Petrol. 42 (8), 1547–1565. https://doi.org/10.1093/petrology/42.8.1547.
Jackson, S.E., Pearson, N.J., Griffin, W.L., Belousova, E.A., 2004. The application of laser ablation-inductively coupled plasma-mass spectrometry to in situ U-Pb zircon geochronology. Chem. Geol. 211, 47–69. https://doi.org/10.1016/j.chemgeo.2004.06.017.
Jacobsen, S.B., Wasserburg, G.J., 1984. Sm-Nd evolution of chondrites and achondrites. Earth Planet. Sci. Lett. 67, 137–150. https://doi.org/10.1016/0012-821X(84)90109-2.
Johnson, M., Rutherford, M.J., 1989. Experimental calibration of the aluminium-in-hornblende geobarometer with application to Long Valley caldera. Geology 17, 837–841 (10.1130/0091-7613(1989)017<0837:ecotai>2.3.co;2).
Katayama, I., Maruyama, S., Parkinson, C.D., Terada, K., Sano, Y., 2001. Ion micro-probe U-Pb zircon geochronology of peak and retrograde stages of ultrahigh-pressure metamorphic rocks from the Kokchetav massif, northern Kazakhstan. Earth Planet. Sci. Lett. 188, 185–198. https://doi.org/10.1016/S0012-821X(01)00319-3.
Klemd, R., Hegner, E., Bergmann, H., Pfänder, J.A., Li, J.L., Hentschel, F., 2014. Eclogitization of transient crust of the Aktyuz complex during late Palaeozoic plate collisions in the Northern Tianshan of Kyrgyzstan. Gondwana Res. 26, 925–941. https://doi.org/10.1016/j.gr.2013.08.018.
Kober, B., 1986. Whole-grain evaporation for $^{207}Pb/^{206}Pb$ age investigations on single zircons using a double filament thermal ion source. Contrib. Mineral. Petrol. 93, 482–490.
Konopelko, D., Kullerud, K., Apayarov, F., Sakiev, K., Baruleva, O., Krogh, Ravna E., Lepekhina, E., 2012. SHRIMP zircon chronology of HP–UHP rocks of the Makbal metamorphic complex in the Northern Tien Shan, Kyrgyzstan. Gondwana Res. 22 (1), 300–309. https://doi.org/10.1016/j.gr.2011.09.002.
Kotková, J., 2007. High-pressure granulites of the Bohemian Massif: recent advances and open questions. J. Geosci. 52, 45–71. https://doi.org/10.3190/jgeosci.006.
Kovach, V., Degtyarev, K., Tretyakov, A., Kotov, A., Tolmacheva, E., Wang, K., Chung, S., Lee, H., Jahn, B., 2017. Gondwana Res. 47, 28–43. https://doi.org/10.1016/j.gr.2016.09.012.
Kozakov, I.K., 1993. Early Precambrian of Central Asian Orogenic Belt. Nauka, Saint Petersburg, p. 272 (in Russian).
Koziol, A.M., Newton, R.C., 1989. Grossular activity-composition relationships in ternary garnets determined by reversed displaced-equilibrium experiments. Contrib. Mineral. Petrol. 103, 423–433. https://doi.org/10.1007/BF01041750.
Krogh, T.E., 1973. A low-contamination method for hydrothermal decomposition of zircon and extraction of U and Pb for isotopic age determination. Geochim. Cosmochim. Acta 37, 485–494. https://doi.org/10.1016/0016-7037(73)90213–5.
Kröner, A., Windley, B.F., Badarch, G., Tomurtogoo, O., Hegner, E., Jahn, B.M., Gruschka, S., Khain, E.V., Demoux, A., Wingate, M.T.D., 2007. Accretionary Growth and Crust Formation in the Central Asian Orogenic Belt and Comparison with the Arabian-Nubian Shield 181–209 (10.1130/2007.1200(11)).
Kröner, A., Alexeiev, D.V., Mikolaichuk, A.V., Xia, X., Zack, T., Windley, B.F., Sun, M., Rojas-Agramonte, Y., Liu, D., 2009. New Single Zircon Ages of Precambrian and Paleozoic Rocks from the Northern, Middle and Southern Tianshan Belts in Kyrgyzstan. International Workshop on Tectonic Evolution and Crustal Structure of the Tien-Shan Belt and Related Terrains in the Central Asian Orogenic Belt. 30–31. CAIAG, Bishkek, Kyrgyzstan (8–17 June, 2009. Abstract volume).
Kröner, A., Alexeiev, D.V., Hegner, E., Rojas-Agramonte, Y., Corsini, M., Chao, Y., Wong, J., Windley, B.F., Liu, D., Tretyakov, A.A., 2012. Zircon and muscovite ages, geochemistry, and Nd-Hf isotopes for the Aktyuz metamorphic terrane: evidence for an early Ordovician collisional belt in the northern Tianshan of Kyrgyzstan. Gondwana Res. 21, 901–927. https://doi.org/10.1016/j.gr.2011.05.010.
Kröner, A., Alexeiev, D.V., Rojas-Agramonte, Y., Hegner, E., Wong, J., Xia, X., Belousova, E., Mikolaichuk, A.V., Seltmann, R., Liu, D., Kiselev, V.V., 2013. Mesoproterozoic (Grenville-age) terranes in the Kyrgyz North Tienshan: zircon ages and Nd-Hf isotopic constraints on the origin and evolution of basement blocks in the Southern Central Asian Orogen. Gondwana Res. 23, 272–295. https://doi.org/10.1016/j.gr.2012.05.004.
Kröner, A., Alexeiev, D.V., Kovach, V.P., Tretyakov, A.A., Mikolaichuk, A.V., Xie, H., Sobel, E.R., 2017. Zircon ages, geochemistry and Nd isotopic systematics for the Palaeoproterozoic 2.3–1.8 Ga Kuilyu Complex, East Kyrgyzstan – The oldest continental basement fragment in the Tianshan orogenic belt. J. Asian Earth Sci. 135, 122–135. https://doi.org/10.1016/j.jseaes.2016.12.022.
Kushev, V.G., Vinogradov, D.P., 1978. Metamorphogenic Eclogites. NAUKA, Novosibirsk. p. 112 (in Russian).
Lanari, P., Vho, A., Bovay, T., Airaghi, L., Centrella, S., 2018. Quantitative Compositional Mapping of Mineral Phases by Electron Probe Microanalyser. Geological Society of London Special Publication https://doi.org/10.1444/SP478.4.
Larionov, A.N., Andreichev, V.A., Gee, D.G., 2004. The Vendian alkaline igneous suite of northern Timan: ion microprobe U–Pb zircon ages of gabbros and syenite. In: Gee, D.G., Pease, V. (Eds.), The Neoproterozoic Timanide Orogen of Eastern Baltica. vol. 30. Geological Society, London, Memoirs, pp. 69–74.
Le Breton, N., Thomson, A.B., 1988. Fluid-absent (dehydration) melting of biotite in metapelites in the early stages of the crustal anatexis. Contrib. Mineral. Petrol. 99, 226–237.
Leake, B.E., Wooley, A.R., Arps, C.E., et al., 1997. Nomenclature of amphiboles: report of the subcommittee on amphiboles of the international mineralogical association, commission on new minerals and mineral names. Can. Mineral. 35, 219–246.
Letnikov, F.A., Kotov, A.B., Sal'nikova, E.B., Shershakova, M.M., Shershakov, A.V., Rizhanova, N.G., Makeev, A.F., 2007. Granodiorites of the Grenville phase in the Kokchetav Block, northern Kazakhstan. Dokl. Earth Sci. 417, 1195–1197. https://doi.org/10.1134/S1028334X07080132.
Levashova, N.M., Mikolaichuk, A.V., McCausland, P.J.A., Bazhenov, M.L., Van der Voo, R., 2007. Devonian paleomagnetism of the North Tien Shan: implications for the

middle–late Paleozoic paleo-geography of Eurasia. Earth Planet. Sci. Lett. 257, 104–120. https://doi.org/10.1016/j.epsl.2007.02.025.
Lexa, O., 2011. PyWerami: Contour/3D Plotting Program for Perple_X WERAMI Data. (Version 2.0.1) [Software]. Available from. http://petrol.natur.cuni.cz/~ondro/pywerami:home.
Li, J.-L., Klemd, R., Gao, J., Jiang, T., Song, Y.-H., 2015. A common high-pressure metamorphic evolution of interlayered eclogites and metasediments from the'ultrahigh-pressure unit' of the Tianshan metamorphic belt in China. Lithos 226, 169–182.
Lu, S.N., Li, H.K., Zhang, C.L., Niu, G.H., 2008. Geological and geochronological evidence for the Precambrian evolution of the Tarim craton and surrounding continental fragments. Precambrian Res. 160, 94–107. https://doi.org/10.1016/j.precamres.2007.04.025.
Ludwig, K.R., 1989. PBDAT for MS-DOS, a Computer Program for IBM-PC Compatibles for Processing Raw Pb- U- Th Isotopic Data: USGS Open-File Report 88–542.
Ludwig, K.R., 2005a. SQUID 1.12 a User's Manual. A Geochronological Toolkit for Microsoft Excel. Berkeley Geochronology Center Spec Pub, p. 22.
Ludwig, K.R., 2005b. User's Manual for ISOPLOT/Ex 3.22. A Geochronological Toolkit for Microsoft Excel. Berkeley Geochronology Center Spec Pub, p. 71.
Ludwig, K.R., 2008. Isoplot V. 4.15: a Geochronological Toolkit for Microsoft Excel. Special Publication, No. 4. 76. Berkeley Geochronology Center.
Ludwig, K., 2012. Isoplot/Ex, Rev. 3.75. A Geochronological Toolkit for Microsoft Excel. 5. Berkeley Geochronology Center Spec. Publ.
Mattinson, J.M., 1994. A study of complex discordance in zircons using step-wise dissolution techniques. Contrib. Mineral. Petrol. 116, 117–129.
Meyer, M., Klemd, R., Konopelko, D., 2013. High-pressure mafic oceanic rocks from the Makbal complex, Tianshan Mountains (Kazakhstan & Kyrgyzstan): Implications for the metamorphic evolution of a fossil subduction zone. Lithos 177, 207–225. https://doi.org/10.1016/j.lithos.2013.06.015.
Mossakovsky, A.A., Ruzhentsev, S.V., Samygin, S.G., Kheraskova, T.N., 1993. Central Asian fold belt: geodynamic evolution and history of formation. Geotectonics 6, 3–33.
Nedovizin, A.A., 1961. To the stratigraphy of the Akzhal formation of the Chu-Ili Mountains. Izvestiya AN KazSSR. Series geod. 2, 26–34 (in Russian).
Nesbitt, H.W., Young, G.M., 1982. Early Proterozoic climates and plate motions inferred from major element chemistry of lutites. Nature 299, 715–717. https://doi.org/10.1038/299715a0.
Nesbitt, H.W., Young, G.M., 1984. Prediction of some weathering trends of plutonic and volcanic rocks based on thermodynamic and kinetic considerations. Geochim. Cosmochim. Acta 48, 1523–1534. https://doi.org/10.1016/0016-7037(84)90408-3.
O'Brien, P.J., Rötzler, J., 2003. High-pressure granulites: formation, recovery of peak conditions and implications for tectonics. J. Metamorph. Geol. 21, 3–20. https://doi.org/10.1046/j.1525-1314.2003.00420.x.
O'Brien, P.J., Vraná, S., 1995. Eclogites with a short-lived granulite facies overprint in the Moldanubian Zone, Czech Republic: petrology, geochemistry and diffusion modelling of garnet zoning. Int. J. Earth Sci. 84 (3), 473–488.
Okamoto, K., Liou, J.G., Ogasawara, Y., 2000. Petrology of the diamond-grade eclogite in the Kokchetav Massif, northern Kazakhstan. Island Arc 9, 379–399. https://doi.org/10.1046/j.1440-1738.2000.00284.x.
Orozbaev, R.T., Takasu, A., Bakirov, A.B., Tagiri, M., Sakiev, K.S., 2010. Metamorphic history of eclogites and country rock gneisses in the Aktyuz area, Northern Tien-Shan, Kyrgyzstan: a record from initiation of subduction through to oceanic closure by continent-continent collision. J. Metamorph. Geol. 28, 317–339. https://doi.org/10.1111/j.1525-1314.2010.00865.x.
Pearce, J.A., Harris, N.B.W., Tindle, A.G., 1984. Trace element discrimination diagrams for the tectonic interpretation of granitic rocks. J. Petrol. 25, 956–983. https://doi.org/10.1093/petrology/25.4.956.
Perchuk, A.L., Lavrent'eva, I.V., 1983. Experimental investigation of exchange equilibria in the system cordierite-garnet-biotite. In: Saxena, S.K. (Ed.), Kinetics and Equilibrium in Mineral Reactions. Advances in Physical Geochemistry 1, pp. 199–240.
Pilitsyna, A.V., Tretyakov, A.A., Degtyarev, K.E., Cuthbert, S.J., Batanova, V.G., Kovalchuk, E.V., 2018a. Eclogites and garnet clinopyroxenites in the Anrakhai complex, Central Asian Orogenic Belt, Southern Kazakhstan: P-T evolution, protoliths and some geodynamic implications. J. Asian Earth Sci. 153, 325–345. https://doi.org/10.1016/j.jseaes.2017.03.027.
Pilitsyna, A.V., Tretyakov, A.A., Degtyarev, K.E., Alifirova, T.A., Batanova, V.G., Cuthbert, S.J., Kovalchuk, E.V., Ermolaev, B.V., 2018b. Multi-stage metamorphic evolution and protolith reconstruction of spinel-bearing and symplectite-bearing ultramafic rocks in the Zheltau massif, Southern Kazakhstan (Central Asian Orogenic Belt). Gondwana Res. 64, 11–34. https://doi.org/10.1016/j.gr.2018.06.005.
Powell, R., Holland, T., 1999. Relating formulations of the thermodynamics of mineral solid solutions: activity modeling of pyroxenes, amphiboles, and micas. Am. Mineral. 84, 1–14. https://doi.org/10.2138/am-1999-1-201.
Rojas-Agramonte, Y., Herwartz, D., García-Casco, A., Kröner, A., Alexeiev, D.V., Klemd, R., Buhre, S., Barth, M., 2013. Early Palaeozoic deep subduction of continental crust in the Kyrgyz North Tianshan: evidence from Lu-Hf garnet geochronology and petrology of mafic dikes. Contrib. Mineral. Petrol. 166, 525–543. https://doi.org/10.1007/s00410-013-0889-y.
Rojas-Agramonte, Y., Kröner, A., Alexeiev, D.V., Jeffreys, T., Khudoley, A.K., Wong, J., Geng, H., Shu, L., Semiletkin, S.A., Mikolaichuk, A.V., Kiselev, V.V., Yang, J., Seltmann, R., 2014. Detrital and igneous zircon ages for supracrustal rocks of the Kyrgyz Tianshan and palaeogeographic implications. Gondwana Res. 26, 957–974. https://doi.org/10.1016/j.gr.2013.09.005.
Ryazantsev, A.V., Mikolaychuk, A.V., Tolmacheva, T.Yu., Degtyarev, K.E., Kotov, A.B., Nikitina, O.I., Mamonov, E.P., Zorin, A.E., 2009. Ophiolites and Island-Arc Complexes of Dzhalair-Naiman Zone and Chu-Kendyktas Massifs (Southern Kazakhstan): Structures, Ages and Formation Settings. Geodynamics of Intracontinental Orogens and Geoecological Problems. Moscow – Bishkek. vol. 4C pp. 53–58.
Schmidt, M.W., 1992. Amphibole composition in tonalite as a function of pressure: an experimental calibration of the Al-in-hornblende barometer. Contrib. Mineral. Petrol. 110, 304–310. https://doi.org/10.1007/BF00310745.
Sengör, A.M.C., Natal'in, B.A., Burtman, V.S., 1993. Evolution of the Altaid tectonic collage and Palaeozoic crustal growth in Eurasia. Nature 364, 299–307. https://doi.org/10.1038/364299a0.
Shatsky, V.S., Jagoutz, E., Sobolev, N.V., Kozmenko, O.A., Parkhomenko, V.S., Troesch, M., 1999. Geochemistry and age of ultrahigh pressure metamorphic rocks from the Kokchetav mass if (Northern Kazakhstan). Contrib. Mineral. Petrol. 137, 185–205. https://doi.org/10.1007/s004100050545.
Shu, L.S., Deng, X.L., Ma, D.S., Xiao, W.J., et al., 2011. Precambrian tectonic evolution of the Tarim Block, NW China: new geochronological insights from the Quruqtagh domain. J. Asian Earth Sci. 42, 774–790. https://doi.org/10.1016/j.jseaes.2010.08.018.
Sláma, J., Košler, J., Condon, D.J., Crowley, J.L., Gerdes, A., Hanchar, J.M., Horstwood, M.S.A., Morris, G.A., Nasdala, L., Norberg, N., Schaltegger, U., Schoene, B., Tubrett, M.N., Whitehouse, M.J., 2008. Plešovice zircon—a new natural reference material for U-Pb and Hf isotopic microanalysis. Chem. Geol. 249, 1–35. https://doi.org/10.1016/j.chemgeo.2007.11.005.
Spear, F.S., 1993. (2nd Printing with Corrections 1995). Metamorphic Phase Equilibria and Pressure-Temperature-Time Paths. Mineralogical Society of America, p. 578.
Spear, F.S., Kohn, M.J., 1996. Trace element zoning in garnet as a monitor of crustal melting. Geology 24 (12), 1099–1102 (https://doi.org/10.1130/0091-7613(1996)024<1099:TEZIGA>2.3.CO;2).
Stacey, J.S., Kramers, I.D., 1975. Approximation of terrestrial lead isotope evolution by a two-stage model. Earth Planet. Sci. Lett. 26 (2), 207–221. https://doi.org/10.1016/0012-821X(75)90088-6.
Steiger, R.H., Jager, E., 1976. Subcomission of Geochronology: convension of the use of decay constants in geo- and cosmochronology. Earth Planet. Sci. Lett. 36 (2), 359–362. https://doi.org/10.1016/0012-821X(77)90060-7.
Sun, S.-s., McDonough, W.F., 1989. Chemical and isotopic systematics of oceanic basalts: implications for mantle composition and processes. Geol. Soc. Lond. Spec. Publ. 42, 313–345. https://doi.org/10.1144/GSL.SP.1989.042.01.19.
Tagiri, M., Yano, T., Bakirov, A., Nakajima, T., Uchiumi, S., 1995. Mineral parageneses and metamorphic P-T paths of ultrahigh-pressure eclogites from Kyrgyzstan Tien-Shan. Island Arc 4, 280–292. https://doi.org/10.1111/j.1440-1738.1995.tb00150.x.
Tanaka, T., Togashi, S., Kamioka, H., Amakawa, H., Kagami, H., Hamamoto, T., Yuhara, M., Orihashi, Y., Yoneda, S., Shimizu, H., Kunimaru, T., Takahashi, K., Yanagi, T., Nakano, T., Fujimaki, H., Shinjo, R., Asahara, Y., Tanimizu, M., Dragusanu, C., 2000. JNdi-1: a neodymium isotopic reference in consistency with La Jolla neodymium. Chem. Geol. 168, 279–281. https://doi.org/10.1016/S0009-2541(00)00198-4.
Taylor, S.R., McLennan, S.M., 1985. The Continental Crust: Its Composition and Evolution. Blackwell, Oxford, p. 312.
Togonbaeva, A., Takasu, A., Bakirov, Az.B., Sakurai, T., Tagiri, M., Bakirov, Ap.B., Sakiev, S., 2009. CHIME monazite ages of garnet-chloritoid-talc schists in the Makbal complex, Northern Kyrgyz Tien-Shan: first report of the age of the UHP metamorphism. J. Mineral. Petrol. Sci. 104 (2), 77–81. https://doi.org/10.2465/jmps.081022e.
Tolmacheva, T.Yu, 2014. In: Alekseev, A.S. (Ed.), Biostratigraphy and Biogeography of Ordovician Conodonts of the Western Part of the Central Asian Orogenic Belt. Transactions of VSEGEI. New series 356. VSEGEI, St. Petersburg, p. 264 (in Russian).
Tretyakov, A.A., Kotov, A.B., Degtyarev, K.E., Salnikova, E.B., Shatagin, K.N., Yakovleva, S.Z., Anisimova, I.V., 2011a. The Middle Riphean volcanogenic complex of the Kokchetav massif (northern Kazakhstan): structural position and age substantiation. Dokl. Earth Sci. 438 (5), 644–648. https://doi.org/10.1134/S1028334X11060262.
Tretyakov, A.A., Degtyarev, K.E., Kotov, A.B., Sal'nikova, E.B., Shatagin, K.N., Yakovleva, S.Z., Anisimova, I.V., Plotkina, Y.V., 2011b. Middle Riphean gneiss granites of the Kokchetav Massif (Northern Kazakhstan): Structural position and age substantiation. Dokl. Earth Sci. 440 (4), 511–515. https://doi.org/10.1134/S1028334X11100072.
Tretyakov, A.A., Degtyarev, K.E., Kovach, V.P., Kotov, A.B., Salnikova, E.B., Pilitsyna, A.V., Yakovleva, S.Z., 2016a. The migmatite–gneiss complex of the Chuya–Kendyktas sialic massif (Southern Kazakhstan): Structure and age. Dokl. Earth Sci. 467, 236–240. https://doi.org/10.1134/S1028334X16030156.
Tretyakov, A.A., Degtyarev, K.E., Sal'nikova, E.B., Shatagin, K.N., Kotov, A.B., Ryazantsev, A.V., Pilitsyna, A.V., Yakovleva, S.Z., Tolmacheva, E.V., Plotkina, Y.V., 2016b. Paleoproterozoic anorogenic granitoids of the Zheltav sialic massif (Southern Kazakhstan): Structural position and geochronology. Dokl. Earth Sci. 466 (2), 1–6. https://doi.org/10.1134/S1028334X16010165.
Turkina, O.M., Letnikov, F.A., Levin, A.V., 2011. Mesoproterozoic granitoids of the Kokchetav microcontinent basement. Dokl. Earth Sci. 436, 176–180. https://doi.org/10.1134/S1028334X11020103.
Van Achterbergh, E., Ryan, C.G., Jackson, S.E., Griffin, W.L., 2001. In: Sylvester, P.J. (Ed.), LA-ICP-MS in the Earth Sciences - Appendix 3, Data Reduction Software for LA-ICP-MS. Vol. 29. Mineralogical Association of Canada, St. John's, pp. 239–243 Short Course Volume.
Watson, E.B., Wark, D.A., Thomas, J.B., 2006. Crystallization thermometers for zircon and rutile. Contrib. Mineral. Petrol. 151, 413–433. https://doi.org/10.1007/s00410-006-0068-5.
Whalen, J.B., Currie, K.L., Chappell, B.W., 1987. A-type granites: geochemical characteristics, discrimination and petrogenesis. Contrib. Mineral. Petrol. 95, 407–419. https://doi.org/10.1007/BF00402202.
White, R.W., Powell, R., Holland, T.J.B., 2001. Calculation of partial melting equilibria in the system Na2O-CaO-K2O-FeO-MgO-Al2O3-SiO2-H2O (NCKFMASH). J. Metamorph. Geol. 19, 139–153. https://doi.org/10.1046/j.0263-4929.2000.00303.x.

Whitney, D.L., Evans, B.W., 2010. Abbreviations for names of rock-forming minerals. Am. Mineral. 95, 185–187. https://doi.org/10.2138/am.2010.3371.

Wiedenbeck, M., Alle, P., Corfu, F., Griffin, W.L., Meier, M., Oberli, F., von Quadt, A., Roddick, J.C., Spiegel, W., 1995. Three natural zircon standards for U-Th-Pb, Lu-Hf, trace-element and REE analyses. Geostand. Newslett. 19, 1–23. https://doi.org/10.1111/j.1751-908X.1995.tb00147.x.

Williams, I.S., 1998. U-Th-Pb geochronology by ion microprobe. In: McKibben, M.A., Shanks III, W.C., Ridley, W.I. (Eds.), Applications of Microanalytical Techniques to Understanding Mineralizing Processes. Vol. 7. Reviews in Economic Geology, pp. 1–35. https://doi.org/10.5382/Rev.07.

Windley, B.F., Alexeiev, D., Xiao, W., Kröner, A., Badarch, G., 2007. Tectonic models for accretion of the Central Asian Orogenic Belt. J. Geol. Soc. Lond. 164, 31–47. https://doi.org/10.1144/0016-76492006-022.

Zhang, R.Y., Liou, J.G., Ernst, W.G., Coleman, R.G., Sobolev, N.V., Shatsky, V.S., 1997. Metamorphic evolution of diamond-bearing and associated rocks from the Kokchetav Massif, northern Kazakhstan. J. Metamorph. Geol. 15, 479–496. https://doi.org/10.1111/j.1525-1314.1997.00035.x.

Zhang, C.-L., Zou, H.-B., Li, H.-K., Wang, H.-Y., 2013. Tectonic framework and evolution of the tarim block in NW China. Gondwana Res. 23, 1306–1315. https://doi.org/10.1016/j.gr.2012.05.009.

Zonenshain, L.P., Kuzmin, M.I., Natapov, L.M., 1990. Geology of the USSR: A Plate Tectonic Synthesis. Geodynamics Series. vol. 21. American Geophysical Union. https://doi.org/10.1029/GD021.